

# The Vertical Stellar Kinematics in Face-On Barred Galaxies: Estimating the Ages of Bars

D. A. Gadotti<sup>1</sup> and R. E. de Souza

*Departamento de Astronomia, Universidade de São Paulo, Rua do Matão, 1226,  
05508-090, São Paulo-SP, Brasil*

dimitri@astro.iag.usp.br, ronaldo@astro.iag.usp.br

## ABSTRACT

In order to perform a detailed study of the stellar kinematics in the vertical axis of bars, we obtained high signal-to-noise spectra along the major and minor axes of the bars in a sample of 14 face-on galaxies, and used them to determine the line of sight stellar velocity distribution, parameterized as Gauss-Hermite series. With these data, we developed a diagnostic tool that allows one to distinguish between recently formed and evolved bars, as well as estimate their ages, assuming that bars form in vertically thin disks, recognizable by low values for the vertical velocity dispersion  $\sigma_z$ . Through  $N$ -body realizations of bar unstable disk galaxies we could also check the time scales involved in the processes which give bars an important vertical structure. We show that  $\sigma_z$  in evolved bars is roughly around 100 Km/s, which translates to a height scale of about 1.4 Kpc, giving support to scenarios in which bulges form through disk material. Furthermore, the bars in our numerical simulations have values for  $\sigma_z$  generally smaller than 50 Km/s even after evolving for 2 Gyr, suggesting that a slow process is responsible for making bars as vertically thick as we observe. We verify theoretically that the Spitzer-Schwarzschild mechanism is quantitatively able to explain these observations if we assume that giant molecular clouds are twice as much concentrated along the bar as in the remaining of the disk.

*Subject headings:* galaxies: bulges — galaxies: evolution — galaxies: formation — galaxies: kinematics and dynamics — methods: N-body simulations

---

<sup>1</sup>Present address: Laboratoire d'Astrophysique de Marseille, 2 Place Le Verrier, 13248 Marseille Cedex 04, France

## 1. Introduction

In the last 10 years or so, bars have gradually become much more than just an intriguing dynamical curiosity (as in the pioneering studies of, e.g., Toomre 1963, 1964; Kalnajs 1972) to reveal its major role in the formation and evolution of galaxies. Contributions to this change of perspective came from various different kinds of analysis, and include the realization that bars may induce the formation of spiral arms and rings (e.g., Schwarz 1981; Combes & Gerin 1985; Buta 1986, see also Buta & Combes 1996), an angular momentum transfer to the outer parts of the galaxy, with consequences as an accumulation of gas in the central regions (e.g., Athanassoula 1992a,b; Friedli & Benz 1993, 1995; Sakamoto et al. 1999a,b), sweeping large scale chemical abundance gradients (Martin & Roy 1994; Zaritsky, Kennicutt & Huchra 1994), possibly building a reservoir of AGN fuel (Shlosman, Frank & Begelman 1989; Shlosman, Begelman & Frank 1990), and provoking central bursts of star formation (e.g., Sérsic & Pastoriza 1965, 1967; Carollo et al. 1997; Gadotti & dos Anjos 2001). Moreover, a number of works came to develop a new bulge building scenario in which bars play a fundamental role (e.g., Combes & Sanders 1981; Kormendy 1982; Kormendy & Illingworth 1983; de Souza & dos Anjos 1987; Pfenniger & Norman 1990; Combes et al. 1990; Balcells & Peletier 1994; Kuijken & Merrifield 1995; Norman, Sellwood & Hasan 1996; Courteau, de Jong & Broeils 1996; Peletier & Balcells 1996; Berentzen et al. 1998; Merrifield & Kuijken 1999; Bureau & Athanassoula 1999; Athanassoula & Bureau 1999; Bureau & Athanassoula 2004, see also the recent review by Kormendy & Kennicutt 2004).

In spite of the undisputed major relevance of bars in the evolution of galaxies, and even though one of the major and basic concerns of any physical science is to measure time scales for natural phenomena, we are not aware of any directed and systematic study on the ages of bars. Relevant points in which such a work may have a substantial impact include the models of Bournaud & Combes (2002), in which bars may be destroyed and rebuilt a few times in a Hubble period, the polemic and long sought correlation between the presence of bars and AGN in galaxies (e.g., Mulchaey & Regan 1997; Ho, Filippenko & Sargent 1997a,b; Knapen, Shlosman & Peletier 2000; Laine et al. 2002; Crenshaw, Kraemer & Gabel 2003; Laurikainen, Salo & Buta 2004), the debated frequency of bars at higher redshifts (van den Bergh 2002; Sheth et al. 2003, and references therein; see also Elmegreen, Elmegreen & Hirst 2004; Jogee et al. 2004) and obviously the formation history of galactic bulges.

Essentially, to estimate for how long a bar is evolving in a certain galaxy one has to measure its vertical extent. This follows from the fact that, as was first shown by Combes & Sanders (1981), when bars form in disks they are vertically thin, but the onset of vertical resonances rapidly makes bars grow thicker in this direction. Another possibility is that the hose instability (Toomre 1966; Merritt & Sellwood 1994), that occurs whenever the velocity

dispersion in the vertical direction is 3 times smaller than in the plane of the disk, also plays its role in this context, by raising the vertical extent of the stellar orbits in the bar region. It is now generally agreed that these processes are likely responsible for the existence of the so called boxy/peanut bulges (see Bureau & Freeman 1999). The signature of bars’ ages may thus be acquired from studying the kinematics along their vertical axis, since it is by elevating the velocity dispersion in this direction that bars evolve and grow away from the plane of the disk.

Another subject that belongs to this discussion regards the difficulties encountered, by what has been until recently the standard scenario for bar formation, in trying to explain the existence of bars in galaxies as early–type as lenticulars (see, e.g., Gadotti & de Souza 2003, and references therein). As the velocity dispersion of the stars in the disk rises, it becomes more and more stable against bar formation through the disk instability. Moreover, the presence of a conspicuous bulge also inhibits this instability (Toomre 1981; Sellwood & Moore 1999). However, Athanassoula (2003) shows that the use of an unresponsive rigid halo in the older numerical experiments induced to a wrong conclusion, namely, that a dark matter halo prevents the onset of the bar instability in the disk within. In reality, the opposite is true: the exchange of angular momentum between disk and halo particles is able to produce in fact even *stronger* bars, and might be a necessary ingredient to account for the existence of barred lenticulars. A few other most important details that were not considered before have been introduced by some authors and will be briefly discussed further on.

In this paper, we obtain suitable stellar kinematical parameters to develop a diagnostic tool that enables us to estimate the ages of bars in a sample of 14 face–on galaxies. In §2, we present the sample and the observations done, while in §3 we show how the kinematical parameters were determined, and introduce our method for bar age estimates. Our results are presented in §4. To numerically assess the time scales involved in the vertical growth of bars, and in this way get a deeper understanding on their evolution, several  $N$ –body simulations were performed. These results are presented in §5, along with a brief discussion concerning bar forming scenarios. In §6, we present a discussion on our results, also considering some of the possible implications on our present knowledge about bar formation and evolution. Finally, §7 summarizes this paper by presenting our main conclusions. We used a value for the Hubble constant of  $H_0 = 70 \text{ Km s}^{-1} \text{ Mpc}^{-1}$ .

## 2. Sample and Observations

Relevant properties of the galaxies in our sample are shown in Table 1. While all of them are bright face–on galaxies of the local universe, one can see that our sample spans a

variety of galaxy morphologies. Of the 14 objects there are 10 strongly barred galaxies and 4 weakly barred ones. Moreover, 7 are of types S0 or S0/a, 3 are Sa and there are also 4 Sb galaxies. Also, our sample contains 4 galaxies with an identified companion that may be gravitationally interacting and 5 with non-stellar nuclear activity. This variety is helpful in trying to evaluate clues related, for instance, to the proeminence of the bulge, the bar strength and the gravitational perturbation of a companion. The presence of galaxies with active nuclei might also be relevant to help in understanding the role played by bars in the fueling of this phenomenon.

In Fig. 1 we show images of all the galaxies in our sample. Lines displayed horizontally help seeing to what extent our spectra were taken along the bars' major and minor axes. For instance, one can see that in the case of the SB0 galaxy NGC 4608 the spectra along the bar minor axis are all within the bar, while those from the SBb galaxy NGC 5850 reach the region outside the bar, in the disk.

Our spectra were taken in two different sets of observing runs. One in the North, in the nights of 1999 May 7, and 2000 April 9 to 11, with the 2.3 m University of Arizona Steward Observatory Bok telescope, on Kitt Peak; and the other in the South, in the nights of 2002 March 13 and December 1 to 5, with the 1.5 m European Southern Observatory telescope at La Silla. The instrumental set-ups are, however, similar. In all runs we have used a Boller & Chivens spectrograph, with a spatial resolution of  $0.8''$  per pixel, a grating with a dispersion of  $1 \text{ \AA}$  per pixel, and an instrumental spectral resolution of  $1.1 \text{ \AA}$ , giving a velocity resolution of  $65 \text{ Km/s}$  in the spectral region of the Mg I feature at  $5175 \text{ \AA}$ , that is approximately the center of all spectra taken. The differences between the North and South spectra are the slit width ( $2.5''$  in the North and  $2''$  in the South), the average seeing ( $1.5''$  in the North and  $1.8''$  in the South), and the spectral range (typically  $1000 \text{ \AA}$  in the North and  $2000 \text{ \AA}$  in the South).

The North spectra are composed from four 1800 s exposures with the slit oriented along the bar major axis and two 1800 s exposures with the slit positioned along the bar minor axis. Whereas in the South we have taken, respectively, four 2700 s exposures and two 2700 s exposures. The slit was always centered in the galaxy nucleus. Thus, the spectra along the bars' minor axis have generally a lower signal-to-noise ratio (S/N) than those along the bars' major axis. This is also due to the fact that the surface brightness decreases more quickly along bars' minor axis. Due to the difference in the telescope apertures the South spectra have also a lower S/N than the North spectra, in general, even considering the larger exposure times in the South runs.

We have also obtained spectra for several standard stars in every run. These are standards for spectrophotometry, velocity measurements and to obtain Lick indices, spanning

spectral types from M to O. In the North we observed Feije 34 (spectral type O, Oke 1990), HR 3951 (G3V), 6458 (G0V), 6685 (F2I), 6770 (G8III), 6775 (F7V), 6806 (K2V), and HR 6868 (M1III), HD 89449 (F6IV), 90861 (K2III), 92588 (K1IV), 136202 (F8III-IV), 155500 (K0III) and HD 172401 (K0III). In the South the stars observed were HR 1544 (A1V), 1996 (O9.5V), 3454 (B3V), 2429 (K1III), 2574 (K4III), 4267 (M5.5III), 4657 (F5V), 4995 (G6V), 5019 (G6V), and HR 5568 (K4V), HD 134439 (K0V), 37984 (K1III), 66141 (K2III), 71597 (K2III) and HD 92588 (K1IV). The spectral types are from Hoffleit & Warren (1991).

All spectra were reduced and extracted from the spectral CCD images using the same standard procedures with the ONEDSPEC and TWODSPEC.LONGSLIT tasks from IRAF<sup>2</sup>. Dark current, overscan and bias were treated as in imaging (e.g., Massey 1997), whereas flatfielding required some extra care, that consisted in a response correction of the dome flatfields to eliminate the continuum from the dome diffuse light, and an illumination correction with the twilight sky flatfields (see, e.g., Massey, Valdes & Barnes 1992).

To extract the spectra we used the IRAF KPNOSLIT.APALL task. To assure that there are no relevant geometric distortions in our instrumental set-up, meaning that one single tracing may be used to extract all spectra from the same spectral image, we have verified that the dispersion axis is the same along the spatial axis, i.e., it is parallel in different positions along the slit. For this we have observed the same standard star in 6 different positions along the slit in a single frame and compared the tracing in all positions. The spectra were extracted for each galaxy along the major and minor axes of the bars in the center and in 8 other different positions along the slit length. To minimize the S/N drop in the outer spectra these were obtained from a gradually larger spatial interval. These were centered at  $r = 0''$ ,  $r = 2.05''$ ,  $r = 4.5''$ ,  $r = 11.9''$  and  $r = 19.3''$  at each side of the center of the galaxy along each bar axis, where  $r$  is the galactocentric radius. The full width of these bins are, respectively, 2.4, 4, 7.2, 15.2 and 21.6 arcseconds, approximately. Thus, the spectra at  $r = 0''$ ,  $r = 4.5''$  and  $r = 19.3''$  are adjacent, i.e., there are no pixels between each bin, but also they don't overlap, as well as those at  $r = 2.0''$  and  $r = 11.9''$ . But considering the seeing effects the only two pairs of independent spectra are at  $r = 0''$  and  $r = 11.9''$ , and at  $r = 2.0''$  and  $r = 19.3''$ . As the S/N drops very quickly from the center it was not possible to obtain spectra farther out.

The spurious contribution from the sky was determined with the light in the outskirts of the slit (3' from the center in the North sample and 2' in the South), where the light

---

<sup>2</sup>IRAF is distributed by the National Optical Astronomy Observatories, which are operated by the Association of Universities for Research in Astronomy, Inc., under cooperative agreement with the National Science Foundation.

contribution from the galaxy is much smaller, and subtracted from the data. Emission sky lines that were not eliminated in this step were manually corrected by direct interpolation. This was especially necessary in the North sample due to the proximity of the city of Tucson to the Kitt Peak (see Kennicutt 1992, where relevant sky lines over Kitt Peak are presented). Cosmic rays and bad pixels were also removed with statistical considerations. The extracted spectra were then continuum normalized and calibrated in wavelength. The error in the latter step was verified to be around 10 Km/s in the region of interest (i.e., at about the Mg I feature).

The next and final step was to bring all spectra to the local standard of rest (LSR). This was of course first done with the velocity standard stars [with velocities available in Abt & Biggs (1972) and in the *Astronomical Almanac*], whose corrected spectra were then used to bring the other ones to the LSR. This was done with the cross correlation technique (Tonry & Davis 1979) and the fact that we had spectra available from stars of many different spectral types was helpful in minimizing the errors caused by template mismatch. As the S/N per pixel is an essential parameter in calculating the errors in the derived line of sight velocity distributions (LOSVDs), they were determined for every galaxy spectrum. We found that  $S/N \sim 40 - 50$  in the central regions of the galaxies while it drops to  $S/N \sim 10 - 20$  in the outermost spectra.

In Fig. 2 we show some illustrative examples of the spectra obtained. The two upper panels refer to spectra obtained along the bar major axis of NGC 4608 and NGC 4579, both from the North sample. The lower panel shows spectra obtained along the minor axis of the bar in NGC 1387, from the South sample. It is worth noticing how the higher values for  $\sigma_z$  in the latter produce a larger width in, e.g., the Mg I lines, and the  $H\beta$  and [O III] emission lines in the LINER/Sey 1.9 galaxy NGC 4579, that are particularly strong in the center, as expected.

### 3. Kinematical Parameters and Bar Age Estimates

#### 3.1. Determining the LOSVDs

The method we have chosen to determine the LOSVDs with our data is the line profile fitting in the pixel space through Gauss–Hermite series (van der Marel & Franx 1993). In this case, assuming, as is generally done, that the main difference between the spectrum of a galaxy and that of a suitable template star is due to the stellar velocities in the galaxy (see, e.g., Binney & Merrifield 1998), following a distribution close to a gaussian, one may write the line profile in the galaxy spectrum as a function of the line of sight stellar velocity  $v$ , as:

$$L(v) = \frac{\gamma\alpha(w)}{\sigma} \sum_{j=0}^4 h_j H_j(w), \quad (1)$$

where

$$\alpha(w) = \frac{1}{\sqrt{2\pi}} e^{-w^2/2}, \quad (2)$$

and

$$w \equiv \frac{v - v_0}{\sigma}. \quad (3)$$

In these equations,  $\gamma$  is the parameter that adjusts the line depth,  $\sigma$  is the stellar velocity dispersion (in our case,  $\sigma \approx \sigma_z$ ),  $v_0$  is the average radial velocity of the system (in our case,  $v_0 \approx 0$ ),  $h_j$  are numerical constants, and  $H_j(w)$  are the orthogonal Hermite polynomials (see Abramowitz & Stegun 1965). We may rewrite Eq. (1) as:

$$L(v) = \frac{\gamma\alpha(w)}{\sigma} [1 + h_3 H_3(w) + h_4 H_4(w)], \quad (4)$$

where

$$H_3(w) = \frac{1}{\sqrt{6}} (2\sqrt{2}w^3 - 3\sqrt{2}w), \quad (5)$$

and

$$H_4(w) = \frac{1}{\sqrt{24}} (4w^4 - 12w^2 + 3), \quad (6)$$

as we have truncated the Gauss–Hermite series in the terms of order 4 (higher order terms are not retrieved reliably, in general), and since  $h_0 = H_0(w) = 1$  e  $h_1 = h_2 = 0$  (see van der Marel & Franx 1993).

Thus, to derive the kinematical parameters along the vertical axis in the major and minor axes of the bars of the galaxies in our sample, we have developed an algorithm that may use template spectra of up to 5 different stars to determine from the galaxy spectrum  $\gamma$ ,  $v_0$ ,  $\sigma$ ,  $h_3$  and  $h_4$ . However, to optimize efficiency we have used up to 3 different template stars, verifying that in our case adding more stars would not result in a significant improvement on

the quality of the results. In this way, errors from template mismatch are severely reduced (see, e.g., Rix & White 1992), as our code is also able to determine the contribution of each stellar type to the galaxy spectrum that maximizes the quality of the fit (i.e., minimizes the  $\chi^2$  value). As shown by van der Marel & Franx (1993) this method here employed minimizes the correlation between the errors in the different kinematical parameters that determine the line profile, which makes the error evaluation safer. Moreover, these authors also show that it is less sensible to template mismatch, as the line profile may fit into the small differences of the spectral properties of the template stars and the galaxy, through adjusts in the higher order moments of the Gauss–Hermite series. Hence, the relevant kinematical parameters we have determined for each galaxy spectrum obtained are  $\sigma_z$  and the third and fourth order moments of the LOSVD parameterized as Gauss–Hermite series,  $h_3$  (the skewness of the velocity distribution) and  $h_4$  (its kurtosis). This was done twice for each spectrum, since, to check the consistency of our results, we have also parameterized the LOSVDs with pure gaussians, i.e., with  $h_3 = h_4 = 0$ .

Figure 3 illustrates how  $h_3$  and  $h_4$  modify the shape of the distribution. As can be seen,  $h_3$  is responsible for asymmetric deviations. A negative value for  $h_3$  means that there is an excess of stars whose velocities are lower than the average system velocity, while the opposite is of course true for a positive  $h_3$ . This is why an anticorrelation between  $h_3$  and  $v$  is generally found in edge-on galaxies to be a signature of a cold, rapidly rotating system (Fisher 1997; Chung & Bureau 2004). On the other hand, a non-negligible  $h_4$  introduces symmetric deviations. A negative value for  $h_4$  indicates a higher number of stars with line of sight velocities close to the average velocity, turning the LOSVD pointy, whereas a positive value is a sign that the distribution is wider near the average velocity. Note also that typically  $h_3$  and  $h_4$  are very small and in the range  $[-0.1, 0.1]$  and that to retrieve reliable values for these parameters the S/N in the spectrum must be higher than about 50. This means that a meaningful discussion on these deviations in our work can only be done when regarding the central spectra. Even so, it is evident, however, that using a generalized gaussian (Gauss–Hermite series) to parameterize the LOSVDs maximizes the quality of the fit and the reliability on the values of the kinematical parameters.

To certify that our code is able to produce reliable estimates a series of tests was performed. In these tests, a stellar spectrum was artificially red shifted and widened by a known LOSVD, resulting in an artificial galaxy spectrum, having also a spectral resolution of 1 Å and a S/N equal to 30, to match the typical characteristics of the spectra in our sample. For the tests we chose generally K giant stars whose spectra were taken from the Elodie archive, that contains high resolution spectra for many stars (see Prugniel & Soubiran 2001). We then used our algorithm to retrieve the LOSVD from the synthetic galaxy spectrum using as template the stars for which we have obtained the spectra. The results have been always ex-



cellent: the solution found by our code, i.e., the template spectrum dislocated and widened by the determined LOSVD has always been very similar to the original synthetic galaxy spectrum. In any case, when determining every LOSVD in this work we have carefully verified that the solution found is indeed similar to the real galaxy spectrum. Figure 4 shows a clarifying example of the fits produced by our code to the spectrum of NGC 1302 at 2.0'' from the center along its bar major axis. Note, moreover, that, to avoid infinite values for  $v$ , our code truncates it, following the relation  $\langle v_e^2 \rangle = 4\langle v^2 \rangle$ , where  $v_e$  is the escape velocity in virialized systems (see Binney & Tremaine 1987).

It is worth noticing how we have selected the template stars in the running of our code to determine the LOSVDs. We followed a careful criterion to minimize even further errors from template mismatch. For every galaxy spectrum we first ran the code using a single stellar template spectrum. This was done with all stars observed under the same instrumental setup. The star that provides the best fit, i.e., the lower  $\chi^2$ , is the first star selected. After that, we ran the code again using as template spectrum a combination of the spectra from the first selected star and all of the other remaining stars separately. Initially, this combination is an average of both stellar spectra but the algorithm is able to give weights to each spectra in order to achieve better results. Again, the pair of stars that produces the best fit is selected. Finally, the algorithm is applied once again, using the spectra of the stellar pair selected combined with the spectrum of each of the remaining stars, to determine the third suitable template star in the same fashion. Generally, with three stars we have achieved the best  $\chi^2$  but, in some cases, using only two stars produced better results. Only one set of template stars was used to retrieve the LOSVDs from all spectra of a given galaxy, since we have verified that the best set of stars does not change when running the code for spectra taken at different galactocentric distances.

Another cause of uncertainties from template mismatch regards the chemical abundances of the template stars. Although most of the template stars we use are K giant or similar, their metallicity (the [Fe/H] ratio) compared to the solar one ranges from  $-0.62$  (HR 6775) to  $+0.25$  (HR 3951) in the North and  $-1.92$  (HD 134439) to  $+0.07$  (HR 2429) in the South, considering the estimates in Cayrel de Strobel, Soubiran & Ralite (2001). Although we did not find the necessary data in the literature this likely means that our template stars span also a significant range in the [Mg/Fe] abundance ratio. This obviously plays a role in studies like ours where Mg and Fe lines are used to calculate the kinematical parameters. This should be suitable to account for differences in the abundance of the galaxies and the stellar templates. Interestingly, following our scheme to choose the most suitable template spectra, stars with [Fe/H] values too different from solar were not considered suitable by our code. For instance, in the North sample the two most chosen stars were HR 6806 ([Fe/H]  $\approx -0.30$ ) and HR 3951, and in the South sample these were HD 37984 ([Fe/H]  $\approx -0.55$ )

and HR 2574 ( $[\text{Fe}/\text{H}] \approx -0.16$ ), with no significant or systematic differences to galaxies that are early-type or late-type. In fact, one should expect such a result as our measurements concern mostly the central regions of galaxies whose morphological types are also mostly early.

The spectral region used to measure the kinematical parameters of the galaxies in our sample is the one that contains mostly absorption lines from the photosphere of, typically, K giant stars, in the range from, approximately, the Mg I triplet at  $\lambda = 5175 \text{ \AA}$  to the Na I feature at  $\lambda = 5893 \text{ \AA}$ . This region also includes relevant lines in this respect, as the Fe I + Ca I lines at  $\lambda = 5265 \text{ \AA}$  and the Fe lines at  $\lambda = 5328 \text{ \AA}$ . In a significant part of the cases studied here a narrower spectral range was used, that excludes the Na I feature. The H $\alpha$  and [H $\beta$ ] lines, at, respectively  $\lambda = 6563 \text{ \AA}$  and  $\lambda = 4861 \text{ \AA}$ , were excluded from the analysis as to avoid spurious results from the complicated emission from gas. In the cases of galaxies with active nuclei, emission lines like, e.g., [O III] ( $\lambda = 5007 \text{ \AA}$ ) were automatically excluded from the analysis by our code, that is able to ignore lines that are too discrepant in the galaxy and template spectra. Nonetheless, we mention a potential source of uncertainty in the spectra of galaxies that present a strong [N I] emission line (the doublet at  $\lambda\lambda 5198, 5200 \text{ \AA}$ ), such as NGC 4579 (see Fig. 2). As shown by Goudfrooij & Emsellem (1996) this feature may affect line strength measurements of the Mg I triplet. Three other galaxies in our sample show also this [N I] emission line: NGC 2665, 4984 and NGC 5701. Although LINERs, the spectra of NGC 1326 and NGC 4314 present only a small feature, while in that of NGC 4394 we have not detected the line. Inspecting our results we find no clear systematic trends regarding this issue.

### 3.2. The Ages of Bars

Having measured the value for  $\sigma_z$  along the major and minor axes of the bars in our galaxy sample, we are ready now to, as in a first order approach, distinguish recently formed and evolved bars. But before going on, let us discuss what one expects to find. We argue that to make this distinction one has to rely not only on the value of  $\sigma_z$  in the bar, but also on its radial behavior in both axes, since the contribution from the bulge and the disk must also be considered. Being a stellar system supported by pressure, bulges will, in general, contribute to a rise in the stellar velocity dispersion in the center, irrespective of the bar age. On the other hand, since in some cases the outer spectra along the bar minor axis reach areas where we are essentially measuring the value for  $\sigma_z$  without relevant contributions from the bar and the bulge, i.e., the vertical velocity dispersion in the disk, in these cases, a comparison between the values of  $\sigma_z$  in the bar and in the disk is most valuable. It should

also be kept in mind that a significant variation in the velocity dispersion from galaxy to galaxy (even with similar morphological types) is expected.

Delhaye (1965, see also Binney & Merrifield 1998) estimates that  $\sigma_z \sim 15$  Km/s in the solar neighborhood for K giant stars. In general, similar values are found for other spectral types. The velocity dispersion in the radial,  $\sigma_r$ , and azimuthal,  $\sigma_\varphi$ , directions are, respectively,  $\sim 30$  Km/s and  $\sim 20$  Km/s. In fact, in the Galactic disk, typically,  $\sigma_z/\sigma_r \sim 0.5$  and  $\sigma_\varphi/\sigma_r \sim 0.6$ , and thus  $\sigma_r > \sigma_\varphi > \sigma_z$ . As the bar length in the Galaxy is estimated to be around 3 Kpc (Blitz & Spergel 1991; Merrifield 2004), and also considering the study of stellar orbits in disk potentials (Binney & Tremaine 1987), these values are expected to be representative for the outer disk in late-type spiral galaxies (Sb–Sc). As the velocity dispersion in the disk rises inward (van der Kruit & Searle 1981), at a galactocentric distance of about the disk length scale  $h$ , which is  $3.5 \pm 0.5$  Kpc in the Galaxy,  $\sigma_z \sim 30$  Km/s. Typical values for  $\sigma_z$  in the center of this class of galaxies are around 50 Km/s (Bottenga 1993). For lenticular galaxies,  $\sigma_z \sim 100$  Km/s in the center, including the contribution from the bulge (McElroy 1995). Farther out  $\sigma_z \sim 50$  Km/s in lenticulars (Fisher 1997).

We can also make an evaluation of the relation between  $\sigma_z$  and the height scale in the disk. In the epicycle approximation (Binney & Tremaine 1987), the vertical oscillation of the stars in the disk in cylindrical coordinates  $(r, \varphi, z)$  is given by  $\ddot{z} = -\nu^2 z$ , where  $\nu$  is the epicycle vertical frequency, given by:

$$\nu^2 = \left( \frac{\partial^2 \Phi}{\partial z^2} \right)_{(r, z=0)}, \quad (7)$$

where  $\Phi$  is the disk gravitational potential. Also, in a highly flattened system,

$$\frac{\partial^2 \Phi}{\partial z^2} = 4\pi G \rho(r, z). \quad (8)$$

And thus,

$$\nu^2 = 4\pi G \rho(r, z = 0). \quad (9)$$

This means that  $\nu$  depends only on the mass density in the plane of the disk, and that in a recently formed bar, assuming that bars are a global dynamical disk instability, the stars are oscillating with this vertical frequency. For the Galaxy, in the solar neighborhood,  $\nu = (3.2 \pm 0.5) \times 10^{-15} \text{ s}^{-1}$ .

On the other hand, through the reasonable assumption that  $\nu$  is independent of  $z$ , we have:

$$z = z_0 \sin(\nu t + \phi_0), \quad (10)$$

where  $z_0$  is the disk height scale,  $t$  is time, and  $\phi_0$  is a phase constant. This implies in:

$$v_z = \dot{z} = z_0 \nu \cos(\nu t + \phi_0), \quad (11)$$

and

$$\langle v_z^2 \rangle = \sigma_z^2 = \frac{1}{2} z_0^2 \nu^2. \quad (12)$$

Thus, considering the disk of the Galaxy typical,

$$z_0 = \frac{\sqrt{2} \sigma_z}{\nu} = 215 (\sigma_z / 15 \text{ Km s}^{-1}) \text{ pc}. \quad (13)$$

Edvardsson et al. (1993) show that for the thin disk of the Galaxy  $\sigma_z = 18$  Km/s while  $\sigma_z = 39$  Km/s for the thick disk. Following our Eq. (13), this means that  $z_0$  is, respectively, 258 and 559 pc. Hence, stars with low  $\sigma_z$  indeed belong to the disk, whereas values of  $\sigma_z$  as high as about 100 Km/s, that implies in  $z_0 \approx 1.4$  Kpc, are certainly not related to the disk component. It is interesting to note that these results are in agreement with the quasi constancy of  $z_0$  along galactic disks (de Grijs & Peletier 1997; van der Kruit 2002). But note also that the radial rise in  $z_0$  is more expressive in the disks of early-type spirals.

Thus, as we have just shown, by measuring  $\sigma_z$  we can have a direct estimate of the vertical extent of the disk. A recently formed bar, as being part of the disk, still has the kinematical properties that characterize disks, namely a low velocity dispersion, that produces a vertically thin structure, that we can infer by observing low ( $\lesssim 50$  Km/s)  $\sigma_z$  values. As the bar evolves, the already mentioned processes like vertical resonances and the hose instability give the bar a higher vertical extent by raising  $\sigma_z$ . These processes, however, make no changes in the remaining of the disk.

In this way, we are able now to devise prescriptions that will make us able to distinguish between recently formed and evolved bars. The first one is possible if one has measurements of  $\sigma_z$  in the bar and in the disk outside the bar and the bulge. This was possible for a few cases in this study, where the outer spectra taken along the minor axis of the bar reach areas

in the disk where the light from the bar and the bulge makes only a small contribution. By comparing the velocity dispersion in the bar and in the disk, a recently formed bar will have yet disk kinematics, whereas an evolved bar will have a larger  $\sigma_z$  than the disk. In Fig. 5 we show schematically how this comparison may be done. The upper panel is an example of a recently formed bar, while the lower one shows the signature of an evolved bar.

Since obtaining kinematical data for the fainter parts of the disk of galaxies is very telescope time demanding, in most of the cases the outer spectra taken along the bar axes are still within the bar or the bulge, even considering the minor axis. Thus, we often may not have an estimate of  $\sigma_z$  in the pure disk to compare to the one in the bar. Hence, we expect that a young bar has not only a low  $\sigma_z$  but also that its radial profile shows a steep outward fall, as the bulge in the center has a much hotter kinematics. Figure 6(a) shows schematically what would be the expected signature of such a case. On the other hand, an old bar is dynamically hotter than the disk, and is possibly as hot as the bulge, and in such case the  $\sigma_z$  radial profile is somewhat flat [see Fig. 6(d)]. However, we may expect to find cases in which the bulge contribution may be misleading. Especially for late-type galaxies, whose bulges may be substantially dynamically colder than average, even a young bar may display a fairly flat  $\sigma_z$  profile, as we show in Fig. 6(b). Furthermore, for the early-type galaxies with their very hot bulges, an evolved bar may show up a steep  $\sigma_z$  profile as can be seen in Fig. 6(c).

Having set up the prescriptions to distinguish young and old bars we postpone to §§5 and 6 the step further of evaluating how much older than young are evolved bars. Instead, in the next section we present the results obtained with the spectra taken in this study.

## 4. Results

The  $\sigma_z$  radial profiles along the bar major and minor axes of the galaxies in our sample are shown in Fig(s). 7 and 8 for the South and North samples, respectively. The reason for a few empty panels in these figures is that we unfortunately were not able to make measurements along the minor axis of the bars in NGC 4984 and NGC 5383. Although we do not present and discuss our results concerning  $h_3$  and  $h_4$ , since the errors on these number estimates render them too unreliable, the fact that similar results are obtained from both parameterizations (i.e., pure gaussian and Gauss–Hermite series) is encouraging. In order to properly analyse these profiles, and try to evaluate which bars are young and which are not, it is also important to know over which radial range the bulge dominates the emitted light and where the light is dominated by the bar or the disk, whose kinematics we want to measure. To determine this we used the ALADIN interactive sky atlas (Bonnarel et al. 2000)

with optical images publicly available through NED. As estimates like these are somewhat subjective we did not try to establish them too precisely. Nonetheless, these estimates serve indeed to our goals. Also, the values referring to the bulge, in particular, mean where its light dominates over that from the bar (and hence the measured kinematics) rather than been its length properly<sup>3</sup>. The results are shown in Table 2. Note that our measurements along the bar major axis are always within the bar itself and that the bulge dominates typically the inner 10 to 15 arcsec along both axes. We stress also that since the spectra are extracted from ever increasing radial bins (from the center outward) there is some overlap in radius that makes the transitions between bulge, bar, and sometimes disk, smoother than in reality.

Following the discussion done so far and the results in Fig(s). 7 and 8 it is possible to qualitatively assess bar ages and distinguish between young and old ones. A quantitative approach, however, is highly desirable. Ideally, for this task one would like to have measurements of the stellar vertical velocity dispersion in the disk and in the bar free from *any* light contamination from other structural components, especially the bulge. In this case, a simple comparison between the values of  $\sigma_z$  would reveal how much the bar has vertically evolved from the original disk. Although this is feasible with the slit configuration we used it is virtually impossible with 2-meter class telescopes, since this means obtaining high S/N spectra from very faint parts of galaxies. Nevertheless, with the data presented here we can pursue such endeavor if we carefully take into account the bulge contribution to the recorded light, using our estimates in Table 2. In addition, let us define a fiducial value that represents  $\sigma_z$  in the bar as the average of our farthest measurements along the bar major axis, that for the majority of our galaxies correspond to  $\approx 50\% - 60\%$  of the bar semi-major length,  $\sigma_{z,\text{bar}}$  [column (6) in Table 2]. This choice comes from a compromise between minimizing bulge contamination and considering the galactocentric distances our spectra reach. Similarly, we can define a fiducial  $\sigma_z$  value for the disk. Since galactic disks have generally a gradient in velocity dispersion we choose to take the disk fiducial  $\sigma_z$  at the same galactocentric distance from which  $\sigma_{z,\text{bar}}$  is defined. Only in this way a meaningful comparison of both values can be achieved. Obviously, however, the disk velocity dispersion is taken along the bar *minor* axis, and the galactocentric distance chosen corresponds to about 1 to 2 times the bar semi-*minor* length. Again, we took an average of our measurements at both sides of the center. Column 7 in Table 2 shows the difference between this and  $\sigma_{z,\text{bar}}$ , defined as  $\Delta\sigma_z$ . Hence, with the help of  $\sigma_{z,\text{bar}}$  and  $\Delta\sigma_z$  we can make a more quantitative assessment in order to distinguish young and old bars.

---

<sup>3</sup>Here we have assumed round bulges for the sake of simplicity. The results from a detailed morphological analysis in Gadotti & de Souza (2005) for 7 galaxies in our present sample indicate an average for the central bulge ellipticity  $\approx 0.1$ . Hence this assumption seems to be fairly reasonable to our purposes.

Then, according to our line of reasoning, some clear cases can be identified. One can say with a certain degree of confidence that NGC 1326, NGC 4394 and NGC 5383 harbor recently formed bars. Their results resemble what we would expect based on Fig(s). 5(a) and 6(a) (for NGC 1326 and NGC 5383) and 6(b) (for NGC 4394). Moreover,  $\sigma_{z,\text{bar}} < 40$  Km/s and  $\Delta\sigma_z < 10$  Km/s (although we do not have this parameter for NGC 5383), that in fact point to these bars as being still a vertically thin structure, belonging to the plane of the disk.

Clear instances of evolved bars are the ones in NGC 1302, NGC 1317 and NGC 5850. Their  $\sigma_z$  radial profiles resemble Fig(s). 5(b) and 6(d). These galaxies have  $\sigma_{z,\text{bar}}$  equal to 100, 145 and 60 Km/s. Although the latter value is clearly much lower, this is a result from the fact that NGC 5850 is of a later morphological class than the former galaxies. In fact,  $\Delta\sigma_z \geq 30$  Km/s in the three cases, an evidence that these bars have vertically grown up from their parent disks.

With these clear instances we can identify typical values for  $\sigma_{z,\text{bar}}$  and  $\Delta\sigma_z$  in old and young bars. For the recently formed ones the average of  $\sigma_{z,\text{bar}} \approx 30$  Km/s where this climbs to  $\approx 100$  Km/s for the evolved ones. Similarly,  $\Delta\sigma_z \approx 5$  and 40 Km/s for young and old bars, respectively.

Let us go now to the less clear cases. The behavior of  $\sigma_z$  in NGC 1387 and NGC 1440 shows a relatively steep fall from the center outward in both axes, and their  $\Delta\sigma_z$  values are low, presumably indicating young bars. However, their values for  $\sigma_{z,\text{bar}}$  are too high to be the case of young bars. These are certainly vertically thick and evolved bars, resembling the schema of Fig. 6(c). These are typical cases where the early-type bulge presents a very high velocity dispersion. The low values of  $\Delta\sigma_z$  may likely be explained by light contamination in the bar minor axis from the bulge and the bar even at the outermost spectra. In fact, in these cases, we have no reliable data on the velocity dispersion of the disk alone. Moreover, note that in the outer spectra  $\sigma_z$  is as high as  $\sim 150$  Km/s. It is hard to devise how the global dynamical disk instability alone could be responsible for the bar in these hot disks, even taking into account that a substantial part of this high velocity dispersion comes from the bulge and the bar. NGC 4608 and NGC 5701 are similar cases. The bulge and bar influence may be causing low values for  $\Delta\sigma_z$ , but the high values of  $\sigma_{z,\text{bar}}$  clearly put these bars in the evolved bin. Their bulges are, however, not as dynamically hot as those of NGC 1387 and NGC 1440 and their  $\sigma_z$  radial profiles resemble Fig. 6(d).

The following cases are more doubtful and thus the reader should have in mind that our conclusions on these cases should be taken with care. NGC 4314 has intermediate values for both  $\sigma_{z,\text{bar}}$  and  $\Delta\sigma_z$  and we do not reach far out enough along the bar major axis. However, the  $\sigma_z$  radial profiles along the bar minor axis show an estimate of  $\sigma_z$  in the disk substantially

lower than those that refer to the bar. Taking this single point into account it seems that the more appropriate is to consider its bar an evolved one. It can in fact be an example where bar evolution is at an intermediate stage. NGC 4579 has a  $\sigma_{z,\text{bar}}$  value closer to that of an evolved bar and a  $\Delta\sigma_z$  value typical of a young one. Our farthest measurements, however, clearly indicate that bar and disk have a similar  $\sigma_z$ , at least in their outer parts, which makes us consider this bar as still recently formed. Contamination from bulge light may again be the cause for the high  $\sigma_{z,\text{bar}}$  values. NGC 2665 is a similar case, and the very low and uncertain  $\sigma_z$  estimates in the farthest points along the bar minor axis may be occulting a young bar behind a high value for  $\Delta\sigma_z$ . In fact, the  $\sigma_z$  estimates along the bar minor axis do not agree in the outermost points from each side of the galaxy center. Good spectra taken at farther galactocentric distances certainly avoid and clarify these doubtful cases.

Finally, the case of NGC 4984 is the only one in that we could not arrive to a definite conclusion. The dispersion reach relatively low values but only in one side of the bar. The lack of minor axis spectra also prevents us to reach a conclusion. Note also that the inner structure of this galaxy is complex (see Fig. 1), and that Jungwiert, Combes & Axon (1997) suggest that this galaxy has a secondary bar possibly almost aligned with the primary. This complexity certainly is reflected in our results.

We performed three different statistical tests within the R environment (see <http://www.R-project.org>) to check if in fact the values we obtained for  $\sigma_{z,\text{bar}}$  and  $\Delta\sigma_z$  to young and old bars point to different objects. An unpaired Student t-test gives a 98% probability that what we defined by young and old bars are indeed different populations considering  $\sigma_{z,\text{bar}}$ . Support to this conclusion comes from Kolmogorov-Smirnov and Wilcoxon (or Mann-Whitney) tests. These tests, however, do not find a significant difference between young and old bars if one considers  $\Delta\sigma_z$ . As discussed above, the lack of  $\sigma_z$  measurements far out in the disk (away from the bar and bulge light) for several cases that an old bar is clearly seen from the analysis of  $\sigma_{z,\text{bar}}$  is the likely cause of the latter result. On the other hand, it is evident that the results from these tests considering  $\sigma_{z,\text{bar}}$  agree with the distinction made here between recently formed and evolved bars. In a later stage it would also be interesting to try to identify intermediate cases. Note that tests like these do not take into account the observational error in each single measurement of, e.g.,  $\sigma_{z,\text{bar}}$ . They, however, use the standard deviation from the mean in both samples (in this case, young and evolved bars) to estimate the observational error and then state the statistical significance of the final result, i.e., the difference between the two samples.

In Fig(s). 7 and 8 one can also verify that at least in NGC 4314 and NGC 5850 there is a central drop in the velocity dispersion. Doubtful cases may be NGC 1317, 4394, 4608, and NGC 5701, since the drop, or the constancy, of  $\sigma_z$  is marginally significant. The remaining



majority of the cases show a peak instead, that is more commonly observed. This peculiarity has been also noted by Emsellem et al. (2001) in 3 other cases. This drop may be caused by a recently formed stellar inner disk originated from the funneling of gas to the center by the bar. In this context, it is noticeable that NGC 4314, NGC 4394, and NGC 5850 present indeed inner disks, as we confirm it through a detailed structural analysis in Gadotti & de Souza (2005, hereafter Paper II) using the BUDDA code (de Souza, Gadotti & dos Anjos 2004).

Many examples of measurements of the stellar velocity dispersion in galaxies can be found in the literature but we are not aware of a systematic measure of this physical parameter along face-on bars. Nonetheless, comparisons with previous values may be instructive, even if not exactly relative to a similar study. Corsini et al. (2003) made measurements of the stellar velocity dispersion in NGC 4984 in a manner similar to what we present here. A comparison of the results from both studies shows that the estimates are essentially the same. Fisher (1997) shows estimates for the stellar kinematics of lenticular galaxies. One can verify that his measurements are very similar to ours as his velocity dispersion estimates for, e.g., NGC 3412, 3941 and NGC 4754 (all barred and more or less face-on) range from  $\approx 200$  Km/s in the center to  $\approx 60$  Km/s 20 arcsec away from it. NGC 3941 is an interesting case worthy to be explored in more detail. Not considering that his measurements are at an angle to the bar major axis one could use our analysis to conclude that the bar is evolved, although better estimates for the velocity dispersion in the disk would be necessary to a more clear conclusion. A similar study involving late-type galaxies can be found in Pizzella et al. (2004). Looking their results for galaxies which are reasonably face-on we again find measurements similar to ours. This is the case for NGC 210, 3054, 6878 and NGC 7412, whose stellar velocity dispersion ranges from  $\approx 150$  Km/s in the center to  $\approx 50$  Km/s 25 arcsec away from it, although we would expect somewhat lower values in the disks of the two latter galaxies. Similar results were found for NGC 488 and NGC 2985 (Gerssen, Kuijken & Merrifield 1997; Gerssen, Kuijken, & Merrifield 2000) and in Bottema (1993) one also finds, for the four face-on galaxies in his sample, estimates similar to ours. If one considers that  $\sigma_z/\sigma_\varphi \sim 0.83$  then inspecting the recent measurements of Kregel, van der Kruit & Freeman (2004) one sees that the range in velocity dispersion they observe in the disks in a sample of edge-on late-type galaxies is in agreement with our estimates for both the late-type galaxies in our sample and the early-type ones, whose  $\sigma$  reaches considerably higher values, also in agreement with previous work (see §3.2 above).

Table 2 also shows error estimates for  $\Delta\sigma_z$ . We followed two different methods to determine these errors. In the first one we propagate the error as usually done in error analysis considering the errors from the spectrum fitting, i.e., those errors determined in §3.1, displayed as error bars in Fig(s). 7 and 8. In our second method we do not consider

the uncertainties in the spectrum fitting, but assume that the error in  $\Delta\sigma_z$  is the quadratic mean of the differences between the values of  $\sigma_z$  in the bar and in the disk (that are used to calculate  $\Delta\sigma_z$ ) taken at both of sides of the galaxy center. This sometimes leads to smaller errors. This analysis shows that the relative error in  $\Delta\sigma_z$  is large, as one should expect considering it is a difference between close numbers, each one already bringing along considerable uncertainty, since they are estimated from faint light. The impact of this uncertainty in our division between young and evolved bars must not be exaggerated, however, since this was done taken also into account  $\sigma_{z,\text{bar}}$  and the full  $\sigma_z$  radial profiles.

## 5. The Vertical Thickening of Bars in $N$ -Body Experiments

It is interesting now to compare the results described in the last section with  $N$ -body realizations of the evolution of barred galaxies. This is useful, for instance, to establish the time scales involved in the vertical thickening of bars. Previous studies estimate the time scale for the occurrence of the boxy-peanut morphology, likely a consequence of vertical resonances and/or the hose instability, in the order of 1 Gyr (see, e.g., Combes & Sanders 1981; Combes et al. 1990). But a systematic comparison of the vertical velocity dispersion in observations and simulations has not been done yet. In this section we perform simplistic  $N$ -body experiments on the evolution of pure stellar disks to use as a first-order approach in making this evaluation. A more realistic treatment would involve adding responsive bulge and halo components, which is beyond our present scope. We note, however, that we intend to perform a more thorough and accurate analysis in a future paper. Thus the results from this section must be considered with caution and tested with more realistic experiments. They are, however, useful to obtain an approximate order of magnitude of how much is the age difference between the young and evolved bars identified above, as well as, and this may be even more important, to attest that measurements of the vertical velocity dispersion along bar and disk are, at least qualitatively, useful for bar age estimates, as we propose here.

The experiments were done within the NEMO package (Teuben 1995), and the Barnes & Hut (1986) tree-code was used for force calculation. We used virial units, in which  $G = M = -4E = 1$ , where  $G$  is the gravitational constant,  $M$  is the mass and  $E$  is the total energy of the system. In the runs a constant time step of typically  $2 \times 10^5$  years was employed, giving about  $10^3$  time steps per crossing time in the systems analysed. The optimal softening parameter suggested by Merritt (1996, see also Athanassoula et al. 2000) for  $N = 10^5$ , that is the number of particles we have used typically, is in the range from  $\epsilon \approx 0.01 - 0.05$ , and the latter value was used. This has the intention of minimizing spurious effects caused by the low number of particles, especially two-body relaxation that may heat

and thicken the disk. Finally, the aperture (or tolerance) angle used was always  $\theta = 0.7$ .

The simulated disks are made of responsive particles of equal masses and are exponential and isothermal with a constant height scale (Freeman 1970, 1978; van der Kruit & Searle 1981):

$$\rho_d(r, z) = \frac{M_d}{4\pi R_d^2 z_0} e^{-r/R_d} \text{sech}^2(z/z_0), \quad (14)$$

where  $M_d$  is the disk mass, being  $R_d$  its length scale. In this case, the Toomre  $Q$  parameter, establishing if the disk is unstable to the bar mode instability, is defined as it is done usually:

$$Q \equiv \frac{\sigma_r \kappa}{3.36 G \Sigma}, \quad (15)$$

where  $\kappa$  is the epicycle frequency of the stellar orbits in the plane of the disk, and  $\Sigma$  is the projected mass surface density. Thus, since  $Q \propto \sigma_r = 2\sigma_z \propto \sqrt{\pi \Sigma z_0}$  (see, e.g., van der Kruit 2002), the stability of the disk is set up in the initial conditions for  $z_0$ . In some of the experiments, however, we have directly attributed a constant value to  $Q$  in the initial conditions, aiming to force the bar instability. In the latter case, is the vertical extent of the disk that is determined as a function of the Toomre parameter. A correction for the asymmetric drift was applied in the disks, assuming the Milky Way disk as typical (see Dehnen & Binney 1998).

Several simulations were run as to mimic the 2 Gyr evolution of stellar disks with properties similar to the Milky Way disk (see Binney & Tremaine 1987; Binney & Merrifield 1998), i.e., a mass  $M_d = 6 \times 10^{10} M_\odot$  and length scale  $R_d = 3.5$  Kpc. The height scale varies in the different experiments in the range  $z_0 = 200 - 600$  pc, which, as discussed above, have fundamental influences on the disk stability against bar formation. The center of mass and energy variation were typically of the order of 0.3%.

We now discuss, based on one representative experiment (with  $z_0 = 450$  pc), the onset of the bar instability in galaxies and the vertical thickening of bars. This fiducial calculation has a Toomre parameter in the initial conditions estimated by Eq. (15) that decreases continuously from  $\approx 3$  in the center to  $\approx 1$  at the outermost radii. Figure 9 displays the evolution of the pure stellar disk in that, as expected, a strong bar develops. This happens after  $t = 6 \times 10^8$  yr and spiral arms also appear in the so called grand design morphology. The bar weakens after  $t = 5 \times 10^8$  yr but remains for a similar period, then giving place to an oval bulge-like distortion until the end of the simulation after 2 Gyr. It can be seen clearly in the edge-on projection the vertical heating of the disk and how the weakening of the bar

originates a bulge-like structure, corroborating previous works (see also Debattista et al. 2004). It is, however, still a matter of debate whether bars are robust, perennial galactic components, or may be easy to dissolve with central mass concentrations, as a result of their natural evolution (see Shen & Sellwood 2004).

Figure 10 shows the evolution of the rotation curve in our experiment. This was derived through the simulation of long slit spectroscopy data, using parameters that match the observations we present in §2, in what concerns the slit width and pixel size on the “sky” and the seeing, i.e., spectral and spatial resolution. The same procedures were done to extract radial profiles of the stellar vertical velocity dispersion along the major and minor axes of the bar, which will be presented and discussed shortly. Note that the rotation velocities reached are low due to the fact that we are not including the mass contributions of either bulge or halo. However, the global shape of the rotation curve is similar to what is generally found for real galaxies (e.g., Rubin et al. 1985). Interestingly, although there is no dark matter halo contribution to these curves, they are quite flat: only a hint of a fall is observed in the second row of panels. This is at least partially explained by the fact that the particle distribution in our disk models is truncated at about 10 Kpc, i.e., only  $\approx 3$  length scales (but see Barnes, Sellwood, & Kosowsky 2004).

We have also made some tests with live bulges and rigid halos as to realize more complete and realistic systems, and verified the difficulties encountered by the old bar formation scenario (that based purely on the bar mode disk instability) in explaining the origin of bars in galaxies with kinematically hot disks and conspicuous bulges, as observed barred lenticulars. However, we can identify five possible ways out that need to be fully exploited to salvage the bar mode instability in disks as the origin of bars in galaxies. First, as showed recently by Athanassoula & Misiriotis (2002) and Athanassoula (2002, 2003), the use of rigid halos is misleading, as their simulations with live halos show that the exchange of angular momentum between the disk and the halo may, contrary to expectations led by previous studies, reinforce the bar. Hence, the present standard bar formation scenario adds to the bar mode disk instability the absorption of angular momentum by a responsive halo. Second, as in the scenario of Bournaud & Combes (2002), the infall of gas from the halo in the disk may also create a kinematically cold structure that is bar unstable. Third, as we showed in Gadotti & de Souza (2003), sufficiently eccentric halos can induce bar formation in kinematically hot stellar systems. Finally, we shall also note that tidal interactions may play a relevant role in this context (Noguchi 2000) and the approach of Polyachenko & Polyachenko (2003).

In all our experiments that do not preclude the appearance of a bar, its properties match previous studies, both in theory and observation. For example, all bars develop quickly in

a few times  $10^8$  yr and have a length in the range from  $\approx 4$  to  $\approx 8$  Kpc. We have also estimated the bar pattern rotation velocity to be around  $30 \text{ Km s}^{-1} \text{ Kpc}^{-1}$ , in general.

Concerning the vertical extent of bars, we show in Fig. 11 that, as predicted, bars grow vertically thick as they evolve, producing a structure similar to a bulge seen edge-on, also presenting the characteristic boxy-peanut morphology. At the time this structure is present, the bar no longer belongs to the disk, since the growth in  $\sigma_z$  produces the vertically thick pseudo bulge. Furthermore, our simulations indicate that this morphology develops quickly (in a few dynamical times, i.e., a few times  $10^8$  yr after the formation of the bar) and weakens after  $\sim 1$  Gyr. Thus, the boxy-peanut morphology may be used as an indication of a young bar, i.e., one that has been originated in less than about 1 Gyr ago. Note also that the presence of a pre-existent bulge would turn difficult the proper identification of the boxy-peanut morphology.

However, in our simulations,  $\sigma_z$  in the bar does not exceed 50 Km/s during the boxy-peanut phase and not even after 2 Gyr of bar evolution. This is shown in Fig. 12, where we present the evolution in time of the stellar vertical velocity dispersion along the bar major and minor axes of our numerical experiment. These profiles were derived using the same procedures we used to produce the rotation curves discussed above. Although tentative, this is evidently in contrast to the observations we reported in the previous section, where evolved bars have  $\sigma_z \sim 100$  Km/s. Thus, while the processes that create the boxy-peanut morphology are fast, the one(s) responsible for the *observed* vertically thickening of the bars should happen in a longer timescale.

A qualitative analysis of Fig. 12 proves very useful. In the first panel (at  $t = 0$ ), corresponding to the initial conditions, the kinematics along major and minor axis of the disk should be (nearly) identical (with small differences from statistical fluctuations), as evolution yet did not start. To produce the velocity dispersion radial profile along the minor axis, we introduce an error of 5 degrees in the slit position angle and an error within the seeing in its central position. This allows one to note that indeed the kinematics is similar in both axes, and also to evaluate how these uncertainties, which are often present in real observations, would affect the measurements. At  $t = 200$  the bar is recently formed and, as we argued above, keeps its kinematical properties along the vertical axis similar to those of the disk. At  $t = 400$  and  $t = 600$ , however, the signature of the evolved bar is clear: in the region dominated by the bar (whose semi-major axis length is about 4 Kpc)  $\sigma_z$  is substantially higher than in the bar-free region of the disk. Hence, our simulations give at least a qualitative support to the bar age diagnostic tool we introduced above. If bars are robust they may keep this signature and yet maybe acquire higher values for  $\sigma_z$ , as we discuss in the next section. In our simulation, however, the bar weakened, a process that

starts at  $t = 800$  and goes until  $t = 1000$  giving origin to an unbarred galaxy with a central morphologically bulge-like structure that also resembles bulges from the kinematical point of view.

For the typical distance of the galaxies in our sample ( $cz \sim 1500$  Km/s) 10 arcsec corresponds roughly to 1 Kpc, which means that our spectroscopic measurements presented in §4 go typically as far as about 2 Kpc from the center, where our simulations (Fig. 12) show that a substantial difference in  $\sigma_z$  would be observed between the evolved bar and the disk.

## 6. Discussion

The ages of bars diagnostic we present here allows us to distinguish between young and old bars, but a further question is to know how much is that age difference. The results from the previous sections suggest that it is not only the processes that cause the boxy-peanut morphology that produce bars as vertically thick as observed. This means that the age difference between young and old bars may be significantly in excess of 1 Gyr. We suggest now that another mechanism is taking place during the evolution of the bar, and that it goes on after the vertical resonances and the hose instability end, giving the bar a vertical extent and a  $\sigma_z$  in agreement with what our observations show.

As shown by Spitzer & Schwarzschild (1951, 1953), collisions with giant molecular clouds (GMCs) are able to make the disk gradually hotter and vertically thicker. This is a process that happens in the disk as a whole (e.g., Binney 2001), but we can reasonably assume that these clouds may be more concentrated along the bar than in the remaining of the disk, given that bars are indeed able to collect and funnel the gas present in the disk to the center. If this is true, then the effect of these collisions will be stronger in the bar region of the disk. It should be mentioned also that this effect happens too with any other inhomogeneity in the stellar density distribution.

The variation in the stellar velocities provoked by the impact with GMCs may be written in the impulsive approximation as:

$$(\Delta v)^2 = \left( \frac{2GM}{bv} \right)^2, \quad (16)$$

where  $M$  is the typical GMC mass, and  $b$  is the impact parameter. The succession of several encounters gives origin to a process of diffusion in phase space (Wielen 1977) in the form:

$$d\sigma_z^2 = D(\Delta v_z)dt, \quad (17)$$

where  $D(\Delta v_z)$  is the diffusion coefficient (see Binney & Tremaine 1987), proportional to  $(\frac{M}{bv})^2$ . If  $D(\Delta v_z)$  is constant, then:

$$\sigma_z^2 = \sigma_{0z}^2 + D(\Delta v_z)t, \quad (18)$$

where  $\sigma_{0z}$  is the initial vertical velocity dispersion. Through numerical simulations, Villumsen (1983) showed that the equation above may be parameterized in the form:

$$\sigma_z = \sigma_{0z} \left(1 + \frac{t}{\tau}\right)^n, \quad (19)$$

with  $n = 1/2$  for a random walk diffusion, and where  $\tau$  is a time scale proportional to  $b^2/M^2$ . This value for  $n$  is in agreement with the relation between the velocity dispersion and the age of stars in the solar neighborhood.

Following the results from Villumsen (1983), this process may elevate the velocity dispersion from  $\sigma_z \simeq 5$  Km/s to  $\sigma_z \simeq 25$  Km/s in about 7 Gyr. Assuming that GMCs are accumulated along the bar, and the fact that  $\tau \propto b^2$ , this mechanism may explain the observed vertically thickening of bars in timescales larger than 1 Gyr. If  $b$  along the bar is half the value of  $b$  in the remaining of the disk, resulting from a higher concentration of GMCs in the bar, then in 7 Gyr  $\sigma_z$  in the bar might go from  $\sigma_z \simeq 5$  Km/s to  $\sigma_z \simeq 100$  Km/s, as observed.

If we consider that during the vertical thickening process bars cease to be kinematically cold then we will have to take into account that the diffusion coefficient is not constant and that  $d\sigma^2/dt \propto 1/\sigma$ . This means that the scattering of stars by GMCs get less efficient in time when we have two kinematically distinct components: the cold disk where GMCs fall, and the vertically rising and hotter bar. This is certainly more justified from the theoretical point of view and leads to  $n = 1/3$ , although the resulting differences are small. Following again the results from Villumsen (1983) this means that the bar takes more 1 – 2 Gyr to achieve  $\sigma_z \simeq 100$  Km/s.

The results from the simulations presented in Athanassoula (1992a,b) and Patsis & Athanassoula (2000) may, however, represent a caveat to the analysis above. This is because they show that gas concentrate in relatively narrow strips along the leading edges of bars. If GMCs behave like gas does in their simulations then the consequences on the stellar

dynamics within the bar may be different from what it would be if, as we assumed above, GMCs are uniformly distributed within the bar. One should note however that, although dust lanes tend in fact to delineate strips along the leading edges of bars in real galaxies, there are also many examples of dust patches *across* bars (see, e.g., Sellwood & Wilkinson 1993).

It is worth noticing at this point that in Paper II we have measured the optical colors of bars in a sample of galaxies similar to the one in this work, including 7 galaxies<sup>4</sup> studied here. We found that the average value for B–V in the bars that our diagnostic identify as evolved is 1.1. In contrast, the identified young bars have B–V equal to 0.7. This color difference may be translated to an age difference of the order of 10 Gyr (see, e.g., Tinsley & Gunn 1976; Maraston 1998), even allowing for reasonable differences in the metallicity of the stellar population. Although the age of the stellar population in the bar does not necessarily represent the age of the bar, this result, in agreement of what we found above with the numerical simulations, corroborate our suggestion that the age difference between young and old bars is significantly higher than 1 Gyr. Although we are here neglecting reddening by dust this is justified by the fact that we defined the bar color at its ends where dust effects are minimized. There is also no reason to believe that dust attenuation should be more effective in galaxies with evolved bars rather than in those with recently formed bars. The reader is referred to Paper II to a more detailed discussion on these color comparisons. Interestingly, in this paper we also find that there are no significant differences in the photometric shape of young and old bars. Considering the 7 galaxies in common with the photometric analysis in Paper II, all their bars show a flat surface brightness profile along the major axis, typical of barred galaxies with morphological types earlier than  $\approx$  Sbc (Elmegreen & Elmegreen 1985). The elliptically averaged surface brightness radial profiles of the galaxies also do not show any clear trend amongst young or old bars concerning profiles of Freeman types I and II (Freeman 1970).

Within this line of reasoning the evolved bars we identified in §4 have ages not much lower than the age of the universe and hence have never dissolved nor are recurrent. Obviously, this does not exclude the possibility of recurrent bars in other galaxies, but it also reinforces the results from Shen & Sellwood (2004), who suggest that bar dissolution requires much more mass concentration than observed, and thus that bars are robust.

Using our diagnostic tool we showed in §4 that from the 14 galaxies in our sample, 8 have evolved bars whereas 5 have recently formed bars. This result may also be interpreted

---

<sup>4</sup>These are NGC 4314, 4394, 4579, 4608, 5383, 5701 and NGC 5850 – i.e., the North sample – which give us 3 recently formed bars and 4 evolved ones.



as an observational evidence of the vertical thickening of bars. Evidently, a more direct way to evaluate the vertical structure of bars is by observing them in edge-on galaxies. In this case, however, the proper identification of bars is still difficult and also involves careful and detailed measurements. Furthermore, in edge-on galaxies one is not able to retrieve several fundamental galactic properties and their detailed structural characteristics.

Our ability in estimate the ages of bars is an important step forward in the study of the formation and evolution of galaxies. We can, for instance, determine more precisely what are the time scales in the secular evolution processes related to bars, and if a given barred galaxy have already suffered from them or not. In fact, we see that from the 8 galaxies with evolved bars only two (25%) have AGN, whereas from the 5 galaxies with young bars three (60%) show AGN activity. While this is yet a small number statistics, it indicates that the time scale for the fueling of AGN by bars is short. In this case, one may find a better correlation between the presence of bars and AGN in galaxies if considering only young bars. This result is also corroborated by those from Paper II, that show that the average B–I color in the bars of AGN galaxies is 1.7, while it is 2.1 in galaxies without nuclear activity. One word of caution, however: the significance of these results are debatable since AGN classifications are derived by different authors in different ways.

It is also interesting to note that from the 8 evolved bars, 7 (88%) reside in early-type galaxies (S0–Sa) while only 1 (12%) is in a Sb galaxy. On the contrary, the young bars seem to preferentially inhabit later-type galaxies: from the 5 young bars, 2 (40%) are found in S0–Sa galaxies and 3 (60%) in Sb. This point is further explored in Paper II. It is also important to stress again that these results must be confirmed by studies with much larger samples as the small number statistics here means their statistical significance is low.

## 7. Conclusion

By exploring the predicted vertical thickening of bars during their evolution, through kinematical measurements in the vertical direction of bars in a sample of 14 galaxies, along their major and minor axes, we have developed and introduced a diagnostic tool that allows one to distinguish between recently formed and evolved bars. Using several  $N$ -body realizations of bar unstable disk galaxies, we studied the time scale involved in the vertical evolution of bars, and the conditions necessary to the onset of the bar instability.

We found that bars may be broadly classified between young and old bars, by, essentially, comparing the vertical velocity dispersion in the bar and in the disk in that it formed. Young bars are kinematically similar (in the vertical direction) to the disks they reside in, having a

low vertical velocity dispersion, thus being still a vertically thin structure in the disk. Old bars, however, have values for vertical velocity dispersion significantly higher than those in their disks, and hence are a vertically thick structure that does not belong to the disk anymore.

We present evidences that the time scale for the vertical thickening of bars may be substantially larger than 1 Gyr, and thus that another physical process in addition to the vertical resonances and the hose instability may be also playing a major role in this context. These evidences come, first, from the numerical experiments, that show that even after 2 Gyr of evolution the simulated bars have a vertical velocity dispersion that does not exceed 50 Km/s, whereas in our observed bars we have measured values of the order of 100 Km/s. Second, this result is corroborated by those we present in Paper II, showing that the average color difference between vertically thin and thick bars suggest an age difference of about 10 Gyr. These results reinforce our suggestion that the Spitzer–Schwarzschild mechanism is responsible for the later vertical thickening of bars, since we demonstrated that it can produce the observed values for the vertical velocity dispersion in these longer time scales. Furthermore, our simulations also show that the boxy–peanut morphology appears quickly, in a few dynamical times after the formation of the bar, and also dissolves relatively quickly, after about 1 Gyr, being hence an indication of a recently formed bar.

To estimate the ages of bars is evidently an important goal in the study of the formation and evolution of galaxies, as it has been proved many times now the major role bars play in this matter. In this paper, we already showed and discussed how it can help us to better understand the intricate relationship between bars and the fueling of AGN. In Paper II, we use this tool together with multiband imaging data to explore furthermore the impact of the formation and evolution of bars on the formation and evolution of galaxies. It is highly desirable now to obtain high quality kinematical data along bars in a growing number of galaxies, and also try to extend them to the outer bar and disk limits, especially to avoid the effects of a bulge. While we are now able to separate bars that are recently formed from the ones that have been already evolving for time scales of several Gyr, the next relevant step is to develop a theoretical understanding of the processes involved in the vertical evolution of bars, in order to be able to refine these age estimates.

This work was financially supported by FAPESP grants 99/07492-7 and 00/06695-0. We thank Rob Kennicutt for his kind hospitality during a visit to the Steward Observatory when part of this work was undertaken. It is a pleasure to thank Lia Athanassoula for her detailed reading and comments on a first version of this manuscript, in particular on its theoretical aspects, which helped to improve our work. Comments and suggestions from both the observational and theoretical anonymous referees were invaluable, and helped to

substantially improve the presentation of our results. We would like to thank Peter Teuben for help on using NEMO (<http://bima.astro.umd.edu/nemo/>). This research has made use of Aladin and of the NASA/IPAC Extragalactic Database (NED), which is operated by the Jet Propulsion Laboratory, California Institute of Technology, under contract with the National Aeronautics and Space Administration. This research has also made use of NASA's Astrophysics Data System, the Lyon Extragalactic Data Archive (LEDA, <http://leda.univ-lyon1.fr/>), and of spectral data retrieved from the Elodie archive at the Observatoire de Haute-Provence (OHP, <http://atlas.obs-hp.fr/elodie>). Statistical tests were made within the R environment (<http://www.R-project.org>).

## REFERENCES

- Abramowitz, M., & Stegun, I. A. 1965, Handbook of Mathematical Functions with Formulas, Graphs, and Mathematical Tables, Dover Books on Advanced Mathematics
- Abt, H. A., & Biggs, E. S. 1972, Bibliography of Stellar Radial Velocities (New York: Latham)
- Athanassoula, E. 1992a, MNRAS, 259, 328
- Athanassoula, E. 1992b, MNRAS, 259, 345
- Athanassoula, E. 2002, ApJ, 569, L83
- Athanassoula, E. 2003, MNRAS, 341, 1179
- Athanassoula, E., & Bureau, M. 1999, ApJ, 522, 699
- Athanassoula, E., Fady, E., Lambert, J. C., & Bosma, A. 2000, MNRAS, 314, 475
- Athanassoula, E., & Misiriotis, A. 2002, MNRAS, 330, 35
- Athanassoula, E., & Sellwood, J. A. 1986, MNRAS, 221, 213
- Balcells, M., & Peletier, R. F. 1994, AJ, 107, 135
- Barnes, E. I., Sellwood, J. A., & Kosowsky, A. 2004, AJ, 128, 2724
- Barnes, J., & Hut, P. 1986, Nature, 324, 446
- Berentzen, I., Heller, C. H., Shlosman, I., & Fricke, K. J. 1998, MNRAS, 300, 49
- Binney, J. 2001, ASP Conf. S., 230, 63

- Binney, J., & Merrifield, M. 1998, *Galactic Astronomy*, (Princeton: Princeton University Press)
- Binney, J., & Tremaine, S. 1987, *Galactic Dynamics*, (Princeton: Princeton University Press)
- Blitz, L., & Spergel, D. N. 1991, *ApJ*, 379, 631
- Bonnarel, F., Fernique, P., Bienaymé, O., Egret, D., Genova, F., Louys, M., Ochsenbein, F., Wenger, M., & Bartlett, J. G. 2000, *A&AS*, 143, 33
- Bottema, R. 1993, *A&A*, 275, 16
- Bournaud, F., & Combes, F. 2002, *A&A*, 392, 83
- Bureau, M., & Athanassoula, E. 1999, *ApJ*, 522, 686
- Bureau, M., & Athanassoula, E. 2004, *ApJ*, submitted
- Bureau, M., & Freeman, K. C. 1999, *AJ*, 118, 126
- Buta, R. 1986, *ApJS*, 61, 609
- Buta, R., & Combes, F. 1996, *Fund. Cosmic Phys.*, 17, 95
- Carollo, C. M., Stiavelli, M., de Zeeuw, P. T., & Mack, J. 1997, *AJ*, 114, 2366
- Cayrel de Strobel G., Soubiran C., & Ralite N. 2001, *A&A*, 373, 159
- Chung, A, & Bureau, M. 2004, *AJ*, 127, 3192
- Combes, F., & Elmegreen, B. G. 1993, *A&A*, 271, 391
- Combes, F., Debbasch, F., Friedli, D., & Pfenniger, D. 1990, *A&A*, 233, 82
- Combes, F., & Gerin, M. 1985, *A&A*, 150, 327
- Combes, F., & Sanders, R. H. 1981, *A&A*, 96, 164
- Corsini, E. M., Pizzella, A., Coccato, L., & Bertola, F. 2003, *A&A*, 408, 873
- Courteau, S., de Jong, R. S., & Broeils, A. H. 1996, *ApJ*, 457, 73
- Crenshaw, D. M., Kraemer, S. B., & Gabel, J. R. 2003, *AJ*, 126, 1690
- Debattista, V. P., Carollo, C. M., Mayer, L., & Moore, B. 2004, *ApJ*, 604, L93
- de Grijs, R., & Peletier, R. F. 1997, *A&AL*, 320, L21

- Dehnen, W., & Binney, J. J. 1998, MNRAS, 298, 387
- Delhaye, J. 1965, Galactic Structure, ed. A. Blaauw & M. Schmidt (Chicago: University of Chicago Press)
- de Souza, R. E., & dos Anjos, S. 1987, A&AS, 70, 465
- de Souza, R. E., Gadotti, D. A., & dos Anjos, S. 2004, ApJS, 153, 411
- de Vaucouleurs, G., de Vaucouleurs, A., Corwin, H. G., Buta, R. J., Paturel, G., & Fouque, P. 1991, Third Reference Catalog of Bright Galaxies (New York: Springer-Verlag **(RC3)**)
- Edvardsson, B., Andersen, J., Gustafsson, B., Lambert, D. L., Nissen, P. E., & Tomkin, J. 1993, A&A, 275, 101
- Elmegreen, B. G., & Elmegreen, D. M. 1985, ApJ, 288, 438
- Elmegreen, B. G., Elmegreen, D. M., & Hirst, A. C. 2004, ApJ, 612, 191
- Emsellem, E., Greusard, D., Combes, F., Friedli, D., Leon, S., Pécontal, E., & Wozniak, H. 2001, A&A, 368, 52
- Fisher, D. 1997, AJ, 113, 950
- Freeman, K. C. 1970, ApJ, 160, 811
- Freeman, K. C. 1978, IAU Symp., 77, 3
- Friedli, D., & Benz, W. 1993, A&A, 268, 65
- Friedli, D., & Benz, W. 1995, A&A, 301, 649
- Gadotti, D. A., & de Souza, R. E. 2003, ApJ, 583, L75
- Gadotti, D. A., & de Souza, R. E. 2005, ApJ, submitted (**Paper II**)
- Gadotti, D. A., & dos Anjos, S. 2001, AJ, 122, 1298
- Gerssen, J., Kuijken, K., & Merrifield, M. R. 1997, MNRAS, 288, 618
- Gerssen, J., Kuijken, K., & Merrifield, M. R. 2000, MNRAS, 317, 545
- Goudfrooij, P., & Emsellem, E. 1996, A&A, 306, L45
- Ho, L. C., Filippenko, A. V., & Sargent, W. L. W. 1997a, ApJ, 487, 579

- Ho, L. C., Filippenko, A. V., & Sargent, W. L. W. 1997b, *ApJ*, 487, 591
- Hoffleit D., & Warren W. H. 1991, *The Bright Star Catalogue*
- Jogee, S. et al. 2004, *ApJ*, submitted (astro-ph/0408382)
- Jungwiert, B., Combes, F., & Axon, D. J. 1997, *A&AS*, 125, 479
- Kalnajns, A. J. 1972, *ApJ*, 175, 63
- Kennicutt, R. C. 1992, *ApJS*, 79, 255
- Knapen, J. H., Shlosman, I., & Peletier, R. F. 2000, *ApJ*, 529, 93
- Kormendy, J. 1982, *ApJ*, 257, 75
- Kormendy, J., & Illingworth, G. 1983, *ApJ*, 265, 632
- Kormendy, J., & Kennicutt, R. C. 2004, *ARA&A*, in press
- Kregel, M., van der Kruit, P. C., & Freeman, K. C. 2004, *MNRAS*, 351, 1247
- Kuijken, K., & Merrifield, M. R. 1995, *ApJ*, 443, L13
- Laine, S., Shlosman, I., Knapen, J. H., & Peletier, R. F. 2002, *ApJ*, 567, 97
- Laurikainen, E., Salo, H., & Buta, R. 2004, *ApJ*, 607, 103
- Maraston, C. 1998, *MNRAS*, 300, 872
- Martin, P., & Roy, J. R. 1994, *ApJ*, 424, 599
- Massey, P. 1997, *A User's Guide to CCD Reductions with IRAF*
- Massey, P., Valdes, F., & Barnes, J. 1992, *A User's Guide to Reducing Slit Spectra with IRAF*
- McElroy, D. B. 1995, *ApJS*, 100, 105
- Merrifield, M. R. 2004, *ASP Conf. S.*, 317
- Merrifield, M. R., & Kuijken, K. 1999, *A&A*, 345, 47
- Merritt, D. 1996, *AJ*, 111, 2462
- Merritt, D., & Sellwood, J. A. 1994, *ApJ*, 425, 551

- Mulchaey, J. S., & Regan, M. W. 1997, *ApJ*, 482, L135
- Noguchi, M. 2000, *MNRAS*, 312, 194
- Norman, C. A., Sellwood, J. A., & Hasan, H. 1996, *ApJ*, 462, 114
- Oke, J. B. 1990, *AJ*, 99, 1621
- Patsis, P. A., & Athanassoula, E. 2000, *A&A*, 358, 45
- Peletier, R. F., & Balcells, M. 1996, *AJ*, 111, 2238
- Pfenniger, D., & Norman, C. 1990, *ApJ*, 363, 391
- Pizzella, A., Corsini, E. M., Vega Beltrán, J. C., & Bertola, F. 2004, *A&A*, 424, 447
- Polyachenko, V. L., & Polyachenko, E. V. 2003, *AL*, 29, 447
- Prugniel, Ph., & Soubiran, C. 2001, *A&A*, 369, 1048
- Rix, H-W., & White, S. D. M. 1992, *MNRAS*, 254, 389
- Rubin, V. C., Burstein, D., Ford, W. K., & Thonnard, N. 1985, *ApJ*, 289, 81
- Sakamoto, K., Okumura, S. K., Ishizuki, S., & Scoville, N. Z. 1999a, *ApJ*, 525, 691
- Sakamoto, K., Okumura, S. K., Ishizuki, S., & Scoville, N. Z. 1999b, *ApJS*, 124, 403
- Sandage, A., & Bedke, J. 1994, *The Carnegie Atlas of Galaxies, Vol. 1* (Washington, DC: Carnegie Inst.)
- Schwarz, M. P. 1981, *ApJ*, 247, 77
- Sellwood, J. A., & Moore, E. M. 1999, *ApJ*, 510, 125
- Sellwood, J. A., & Wilkinson, A. 1993, *Rep. Prog. Ph.*, 56, 173
- Sérsic, J. L., & Pastoriza, M. 1965, *PASP*, 77, 287
- Sérsic, J. L., & Pastoriza, M. 1967, *PASP*, 79, 152
- Shen, J., & Sellwood, J. A. 2004, *ApJ*, 604, 614
- Sheth, K., Regan, M. W., Scoville, N. Z., & Strubbe, L. E. 2003, *ApJ*, 592, L13
- Shlosman, I., Begelman, M. C., & Frank, J. 1990, *Nature*, 345, 679

- Shlosman, I., Frank, J., & Begelman, M. C. 1989, *Nature*, 338, 45
- Spitzer, L., & Schwarzschild, M. 1951, *ApJ*, 114, 385
- Spitzer, L., & Schwarzschild, M. 1953, *ApJ*, 118, 106
- Teuben, P. J. 1995, *ASP Conf. Ser.*, 77, 398
- Tinsley, B. M., & Gunn, J. E. 1976, *ApJ*, 203, 52
- Tonry, J., & Davis, M. 1979, *AJ*, 84, 1511
- Toomre, A. 1963, *ApJ*, 138, 385
- Toomre, A. 1964, *ApJ*, 139, 1217
- Toomre, A. 1966, Notes on the 1966 Summer Study Program in Geophysical Fluid Dynamics at Woods Hole Oceanographic Institution, Vol. 1 (Woods Hole: Woods Hole Oceanographic Inst.), 111
- Toomre, A. 1981, *Structure and Evolution of Normal Galaxies*, ed. S. M. Fall & D. Lynden-Bell (Cambridge: Cambridge Univ. Press), 111
- van den Bergh, S. 2002, *AJ*, 124, 782
- van der Kruit, P. C. 2002, *ASP Conf. S.*, 273, 7
- van der Kruit, P. C., & Searle, L. 1981, *A&A*, 95, 105
- van der Marel, R. P., & Franx, M. 1993, *ApJ*, 407, 525
- Villumsen, J. V. 1983, *ApJ*, 274, 632
- Wielen, R. 1977, *A&A*, 60, 263
- Zaritsky, D., Kennicutt, R. C., & Huchra, J. P. 1994, *ApJ*, 420, 87



Table 1. Basic data for all galaxies in our sample.

Name (1)	Type (2)	$D_{25}$ (3)	$\log R_{25}$ (4)	$m_B$ (5)	$cz$ (6)	AGN (7)	Companion (8)
NGC 1302	SB0(r)	3.89	0.02	11.40	1730	...	N
NGC 1317	SABa(r)	2.75	0.06	11.85	1941	...	Y
NGC 1326	SB0(r)	3.89	0.13	11.42	1365	LINER	N
NGC 1387	SAB0(s)	2.82	0.00	11.82	1328	...	Y
NGC 1440	SB0(rs)	2.14	0.12	12.58	1504	...	N
NGC 2665	SBa(rs)	2.04	0.13	12.96	1740	...	N
NGC 4314	SBa(rs)	4.17	0.05	11.22	963	LINER	N
NGC 4394	SBb(r)	3.63	0.05	11.53	772	LINER	Y
NGC 4579	SABb(rs)	5.89	0.10	10.68	1627	LINER/Sey1.9	N
NGC 4608	SB0(r)	3.24	0.08	11.96	1823	...	N
NGC 4984	SAB0(rs)	2.75	0.10	11.80	1243	...	N
NGC 5383	SBb(rs)	3.16	0.07	12.18	2226	...	Y
NGC 5701	SB0/a(rs)	4.26	0.02	11.82	1556	LINER	N
NGC 5850	SBb(r)	4.26	0.06	12.04	2483	...	N

Note. — Columns (1) and (2) show, respectively, the name and the morphological type of the galaxy, while column (3) shows its diameter in arcminutes at the 25 B magnitude isophotal level, and column (4) shows the decimal logarithm of its major to minor axes ratio at the same level. Columns (5) and (6) show, respectively, the apparent B magnitude and the radial velocity in Km/s. All these data were taken from de Vaucouleurs et al. (1991, hereafter RC3). Column (7) presents an AGN classification according to the NASA Extragalactic Database (hereafter NED). In column (8), “Y” means that there is a companion galaxy similar in size physically interacting within 10 arcminutes, while “N” means that there are no companion galaxies. To make this analysis we used the RC3 and the Lyon Extragalactic Data Archive (hereafter LEDA).

Table 2. Relevant properties of bulges and bars of the galaxies in our sample to a proper evaluation of the bar ages from the radial profiles of the vertical velocity dispersion [Fig(s). 7 and 8].

Galaxy NGC (1)	Bulge Major Axis (2)	Bar Major Axis (3)	Bulge Minor Axis (4)	Bar Minor Axis (5)	$\sigma_{z,\text{bar}}$ (Km/s) (6)	$\Delta\sigma_z$ (Km/s) (7)	Error (1) (Km/s) (8)	Error (2) (Km/s) (9)	Bar Age (10)
1302	10	40	10	20	100	28	47	12	old
1317	15	35	15	25	145	57	71	70	old
1326	10	35	10	10	38	8	34	6	young
1387	15	45	15	30	159	2	52	46	old
1440	15	35	15	15	178	2	83	20	old
2665	10	35	10	20	67	32	43	66	young?
4314	10	80	10	15	59 <sup>a</sup>	20	21	32	old?
4394	7	40	7	10	28	0	27	23	young
4579	10	40	10	10	57	6	20	3	young
4608	15	45	15	10	62	9	38	35	old
4984	15	35	...	...	68	...	...	...	...
5383	10	52	...	...	23 <sup>a</sup>	...	...	...	young
5701	15	50	15	10	85 <sup>a</sup>	5	52	7	old
5850	8	72	8	12	60 <sup>a</sup>	33	40	4	old

Note. — Column (1) gives the NGC number of the galaxy while columns (2) through (5) show the apparent length in arcseconds of the semi-major and semi-minor axes of bulges and bars after visual inspection (see text for details). Note that our measurements reach approximately 20 arcseconds from the center. Column (6) gives the vertical velocity dispersion measured along the bar major axis at  $\approx 50\% - 60\%$  of the bar semi-major length, unless when <sup>a</sup> notifies that our spectra do not reach this galactocentric distance. Column (7) gives the difference between columns (6) and  $\sigma_z$  measured in the disk along the bar minor axis at the same galactocentric distance. The values in columns (6) and (7) are averages from both sides of the bar axes. Columns (8) and (9) show error estimates in the values of  $\Delta\sigma_z$  according to two different procedures (see § 4). Finally, column (10) shows whether the galaxy harbor an young or and old bar according to the method and criteria developed here. Doubtful cases are notified.

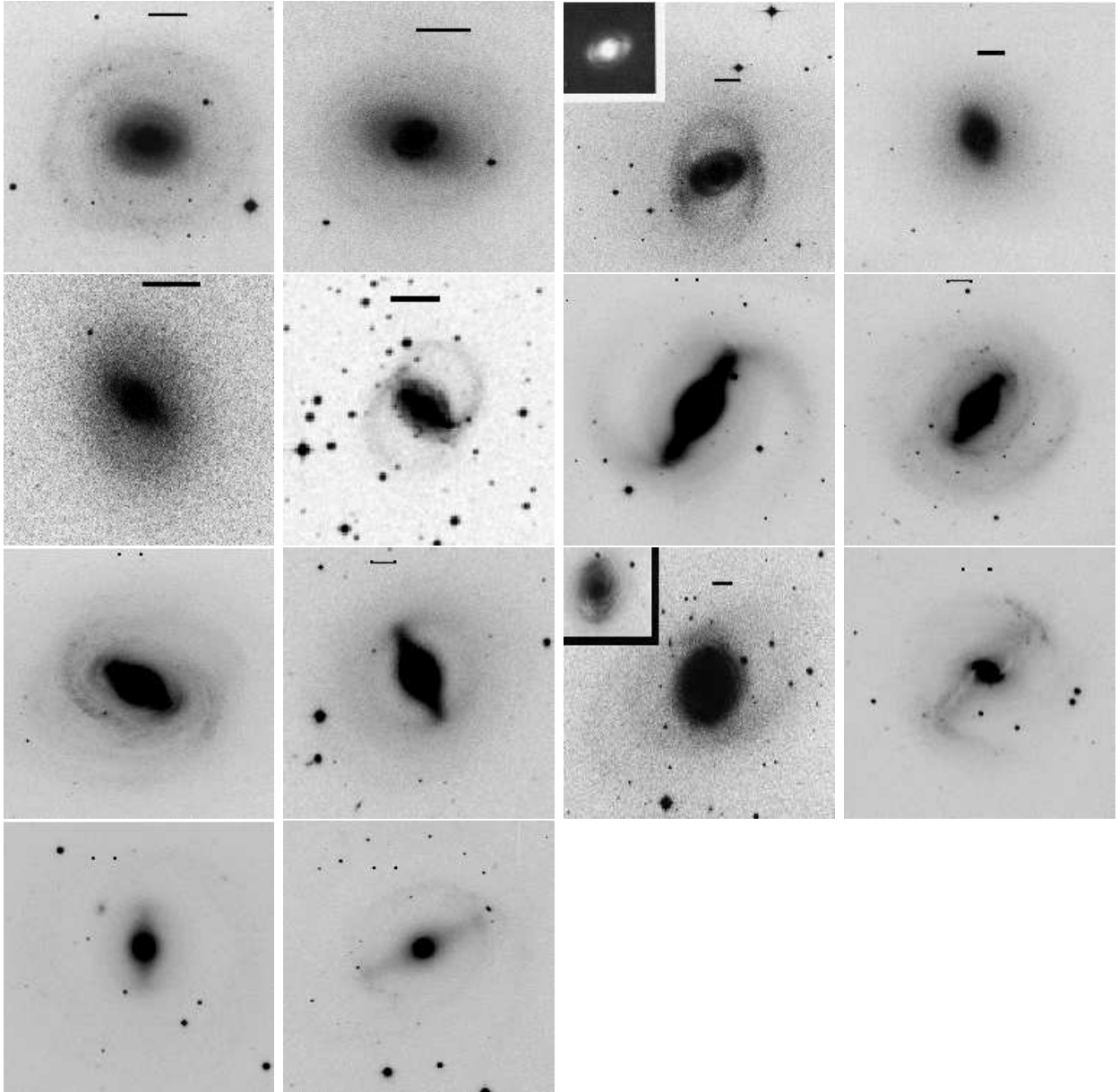


Fig. 1.— All galaxies from our sample. From left to right and from top to bottom: NGC 1302, 1317, 1326, 1387, 1440, 2665, 4314, 4394, 4579, 4608, 4984, 5383, 5701, and NGC 5850. Horizontal lines in each panel have approximately a 20 arcseconds length, except for NGC 2665, where it has 30 arcseconds. These images were taken from the Carnegie Atlas of Galaxies (Sandage & Bedke 1994), the Digitized Sky Survey, and from our own R CCD images (Gadotti & de Souza 2005).

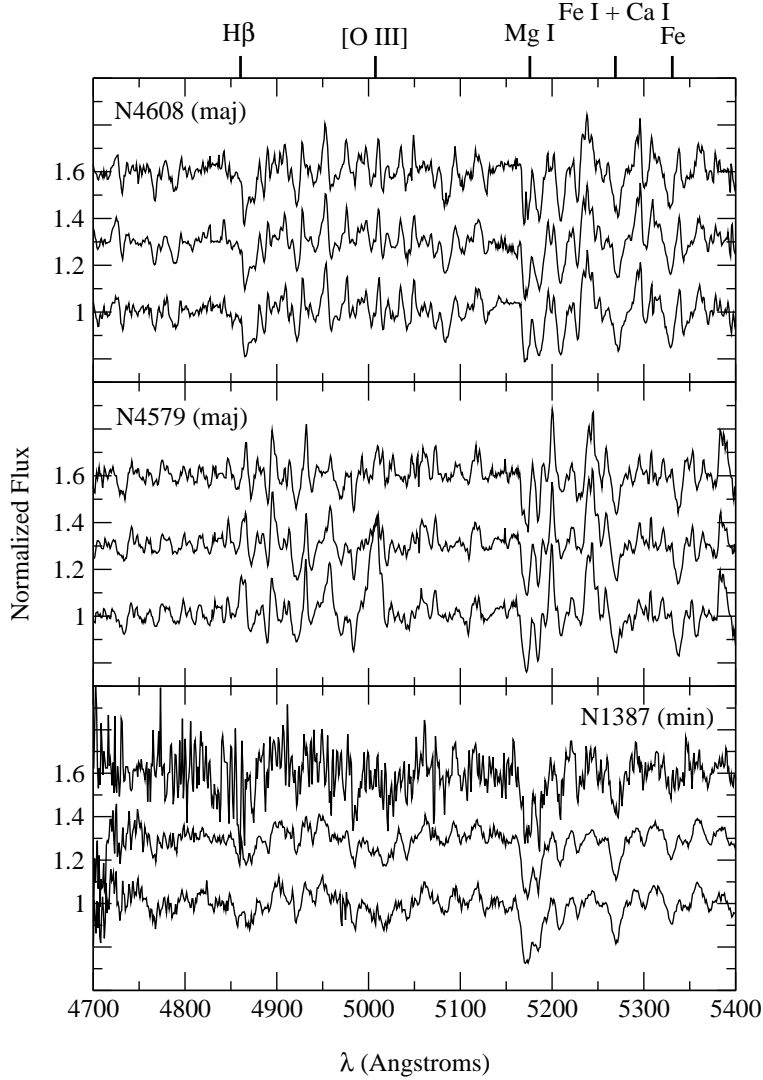


Fig. 2.— Some typical examples of the spectra we have obtained. The two upper panels refer to spectra obtained along the bar major axis of NGC 4608 and NGC 4579, both from the North sample. The lower panel shows spectra obtained along the minor axis of the bar in NGC 1387, from the South sample. For each galaxy, as indicated, the lower spectrum is the central one, while the middle one was extracted at 4.5'' from the center, and the upper one at 19.3''. The latter were artificially dislocated in this figure to avoid crowding. The emission line at  $\lambda \approx 5200 \text{ \AA}$  in NGC 4579 is the [N I] doublet.

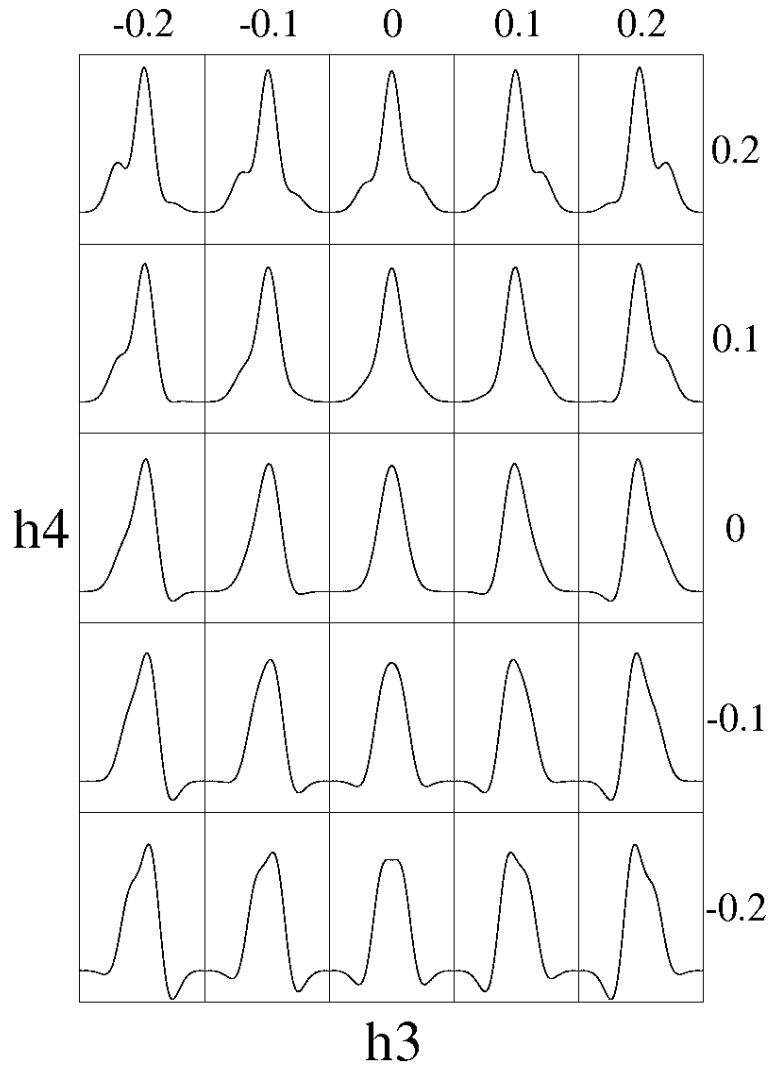


Fig. 3.— A pure gaussian ( $h_3 = h_4 = 0$ ) may suffer asymmetric deviations when  $h_3 \neq 0$  and symmetric deviations when  $h_4 \neq 0$ .

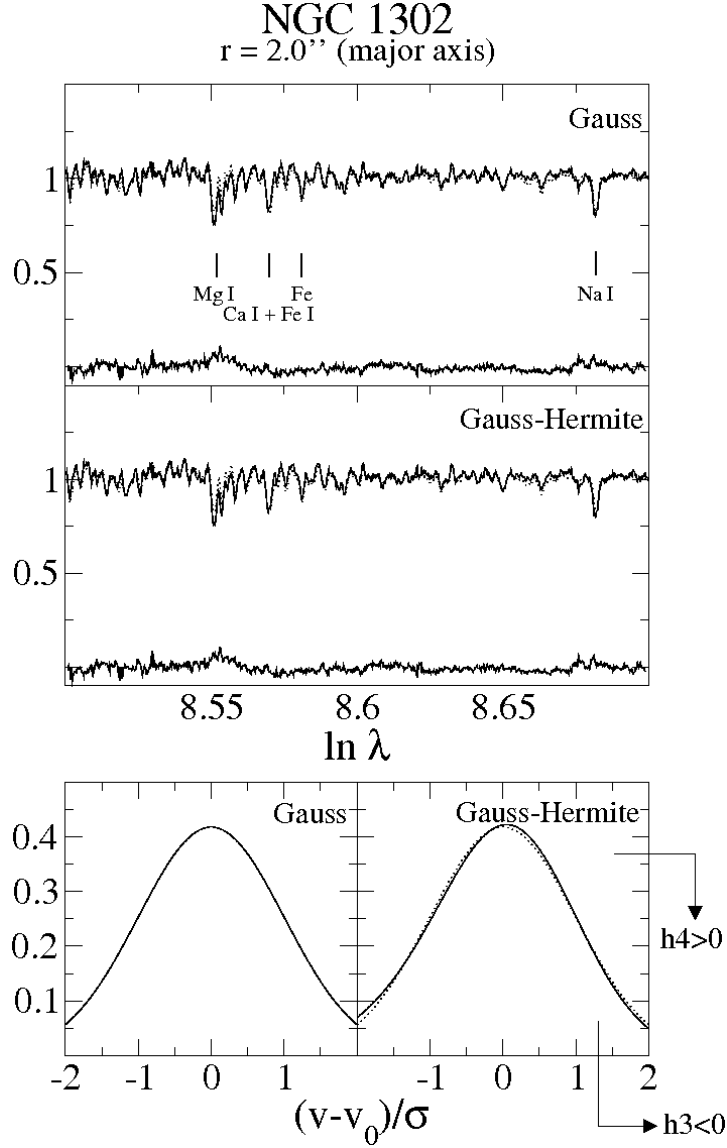


Fig. 4.— An example of the fits generated by our code to retrieve the LOSVDs from the galaxy spectra, in this case NGC 1302 at 2.0'' from the center along its bar major axis. The results from the two parameterizations are shown: the velocity distribution as a pure gaussian (upper panel and lower left panel), and as a generalized gaussian (Gauss–Hermite series, middle panel and lower right panel). The upper and middle panels show the galaxy spectrum (solid line) and the solution found with the template stars and the determined LOSVD (dotted line). Residuals are also shown. The lower panels show the determined LOSVDs. Note the effects of the higher order moments of the generalized gaussian. In the lower right panel the dotted line is a pure gaussian profile for comparison.

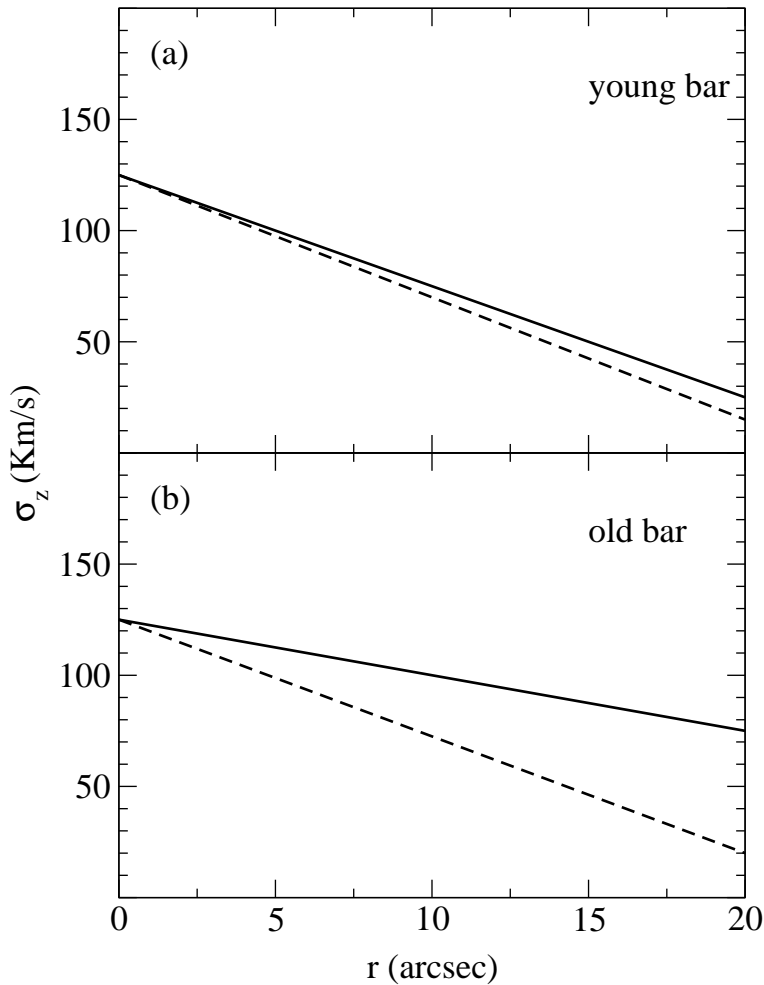


Fig. 5.— If one is able to measure  $\sigma_z$  not only along the bar major axis (solid line) but also in the bar minor axis (dashed line), reaching in the latter case regions in the galaxy dominated only by the disk, i.e., outside the contributions from the bulge and the bar, then a simple comparison of the values of  $\sigma_z$  in the bar and in the disk will suffice to evaluate if the bar is young or old. A young bar (a) has a velocity dispersion yet similar to the one in the disk, whereas an evolved bar (b) has a much higher  $\sigma_z$  than the disk due to its dynamical evolution. Note that the units for the abscissae are of course only meant to represent our study. The location of the different  $\sigma_z$  behaviors will evidently vary in different galaxies.

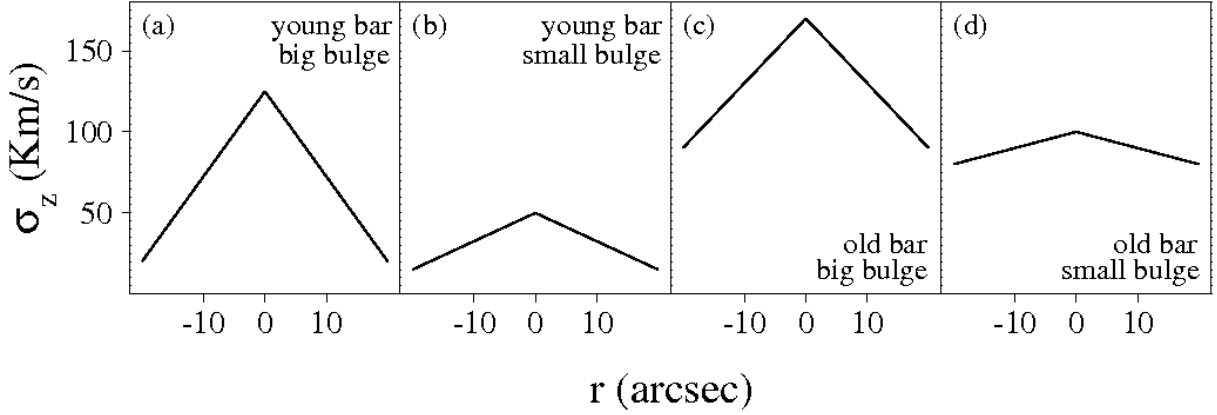


Fig. 6.— Typical radial profiles of  $\sigma_z$  for young and old bars in the presence of a bulge. In most cases, the acquisition of spectra from pure disk regions is very difficult and even the outermost spectra along the minor axis may be still within the bar. In these cases the radial behavior of  $\sigma_z$  is somewhat similar along both the major and minor axes of the bar. The kinematics of the bulge basically affects the central velocity dispersion. The two leftmost panels show examples of recently formed bars, revealed by the low values for  $\sigma_z$  typical of disk stars, while in the rightmost panels the evolved bars may be recognized by values of  $\sigma_z$  that can not be ascribed to a disk. In (a) and (c), however, the bulge is dynamically hotter than the bar, even an evolved one. In (b) and (d), on the other hand, the kinematics of the bulge and the bar are similar, and this may be true for a young or for an old bar. Morphological differences may also account for this different behaviors, as bulges of earlier-type galaxies have a larger velocity dispersion. Note that the units for the abscissae are of course only meant to represent our study. The location of the different  $\sigma_z$  behaviors will evidently vary in different galaxies.



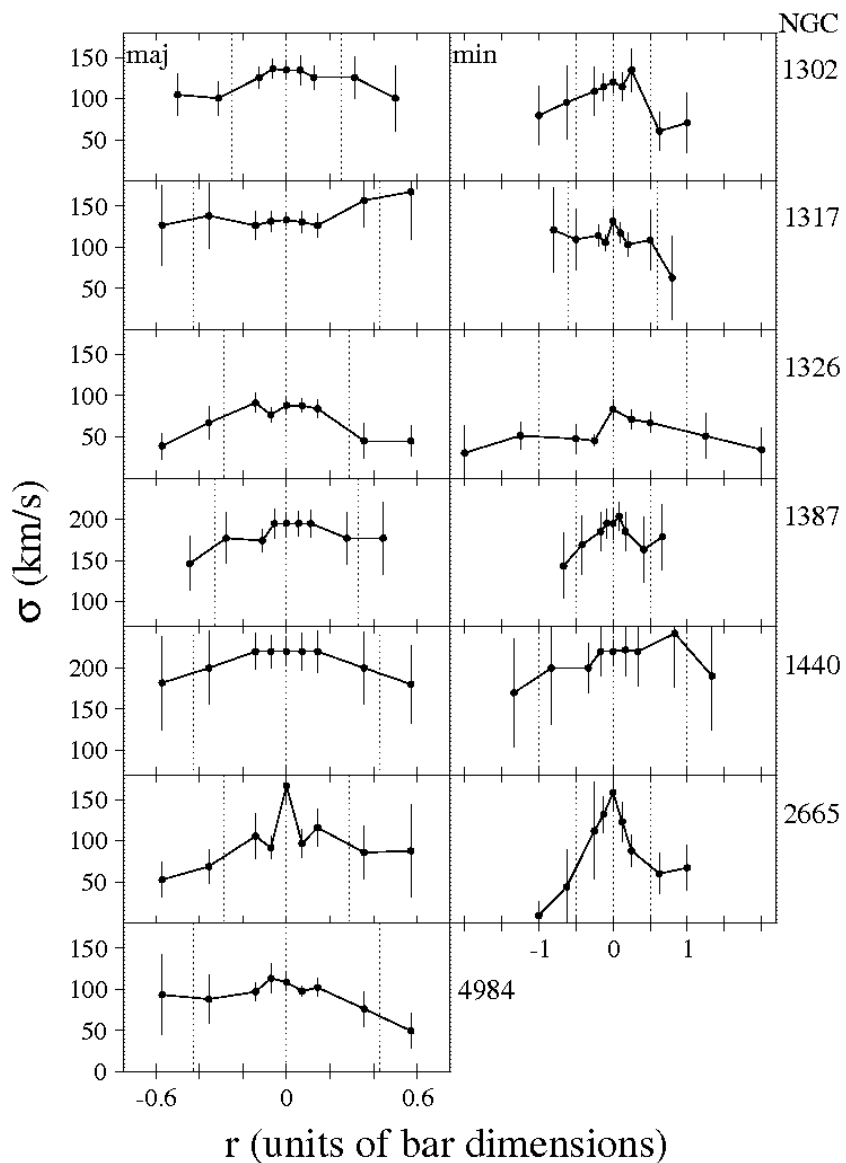


Fig. 7.— Vertical velocity dispersion radial profiles for the galaxies in our South sample along the major and minor axes of the bars, as displayed. The figures refer to a parameterization of the LOSVDs as a pure gaussian, but similar results were obtained when we made use also of the  $h_3$  and  $h_4$  higher order moments of the Gauss–Hermite series. Dotted lines mark the center and the region where the emitted light is dominated by the bulge. Units in the abscissae are normalized by the bar semi-major and semi-minor axes.

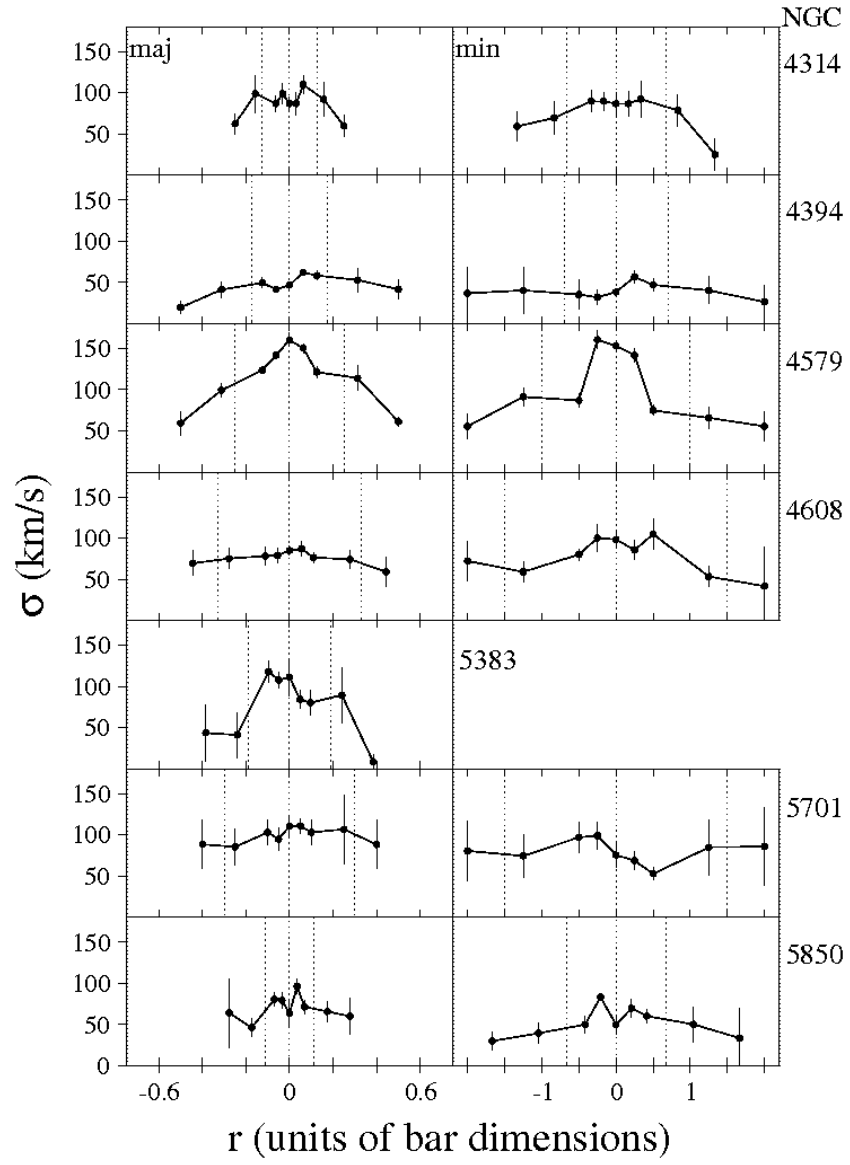


Fig. 8.— Same as Fig. 7 but for the North sample.

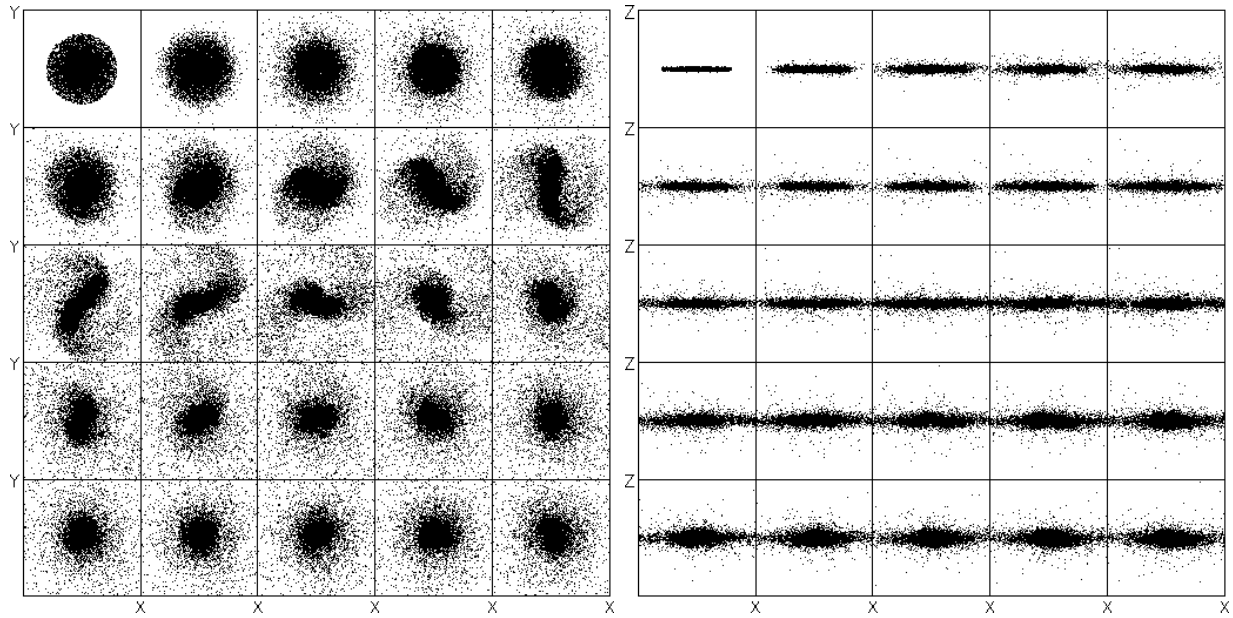


Fig. 9.— Formation of the grand design morphology in the evolution of a pure stellar disk seen face-on (left) and edge-on (right). The top leftmost panels show the initial conditions, whereas the bottom rightmost panels refer to  $t = 1.9$  Gyr of evolution. The time interval between each panel is  $t = 8 \times 10^7$  yr and its physical dimension is 16 Kpc. Only 10% of the particles in this simulation are shown.

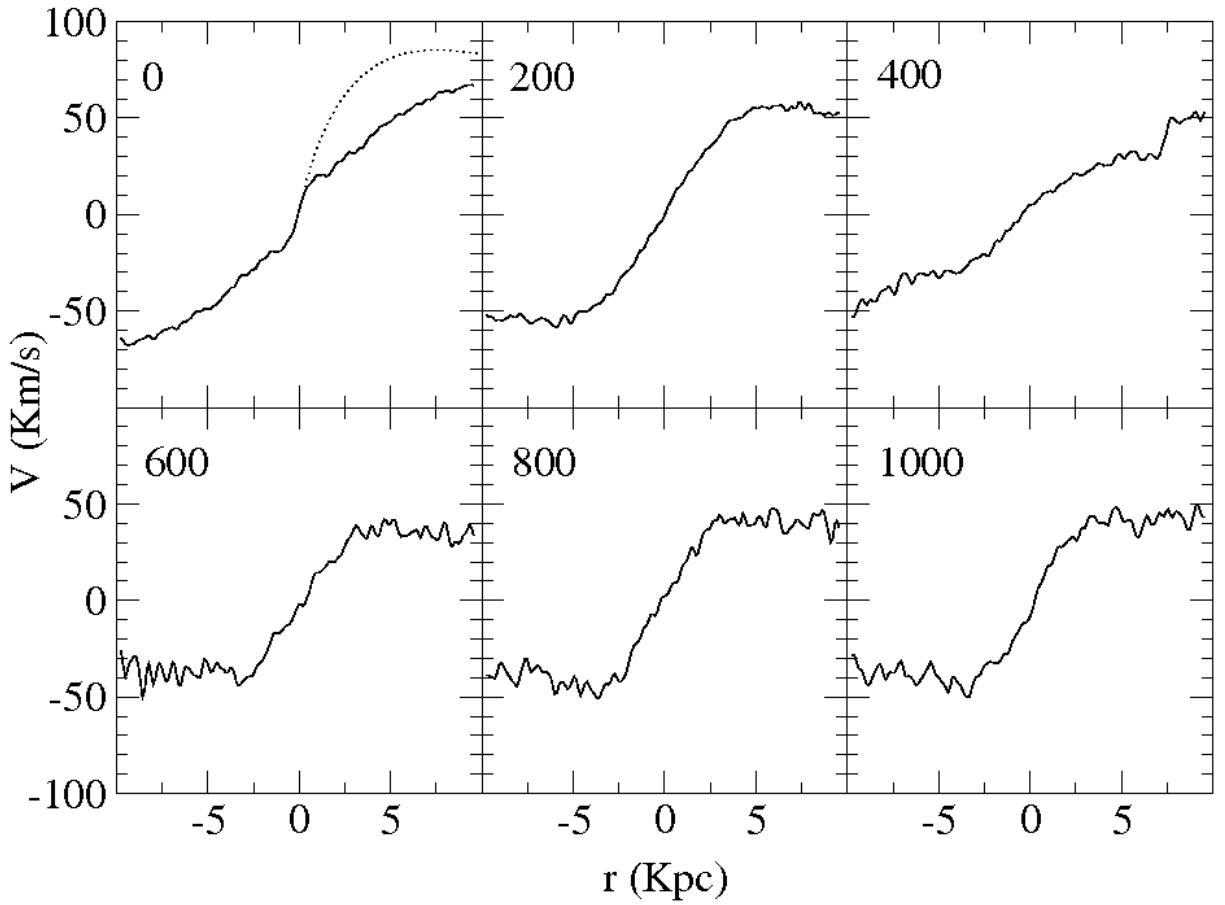


Fig. 10.— Evolution in time of the rotation curve, as measured from simulated long slit spectroscopy, in our representative stellar disk numerical simulation. The corresponding times in virial units are displayed in the top left of each panel. The last panel corresponds to 2 Gyr of evolution. The dotted line in the first panel is the initial circular speed curve, for comparison.

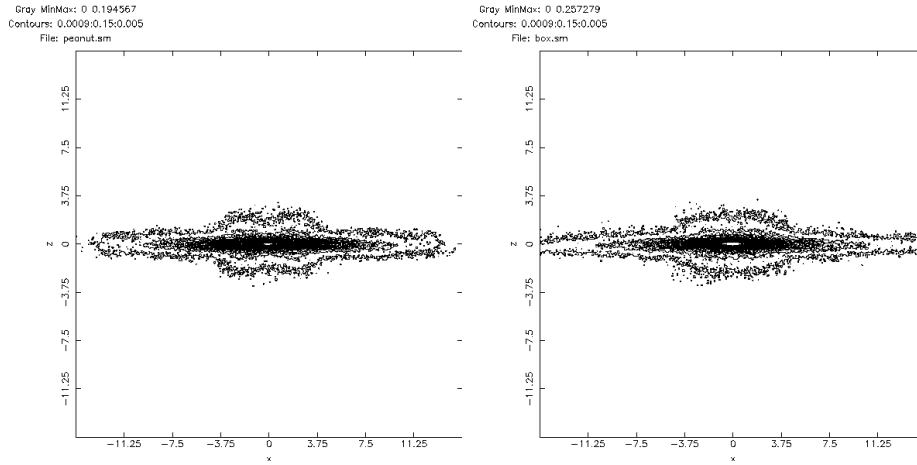


Fig. 11.— Isodensity contours in our fiducial numerical experiment seen edge-on in  $t = 3.6 \times 10^8$  yr (left) and in  $t = 4 \times 10^8$  yr (right). Note that the peanut morphology appears when the line of sight is closer to a perpendicular orientation with respect to the bar major axis (left), whereas the boxy morphology appears when the line of sight is closer to a parallel orientation with respect to the bar major axis (right). Dimension units are 650 pc.

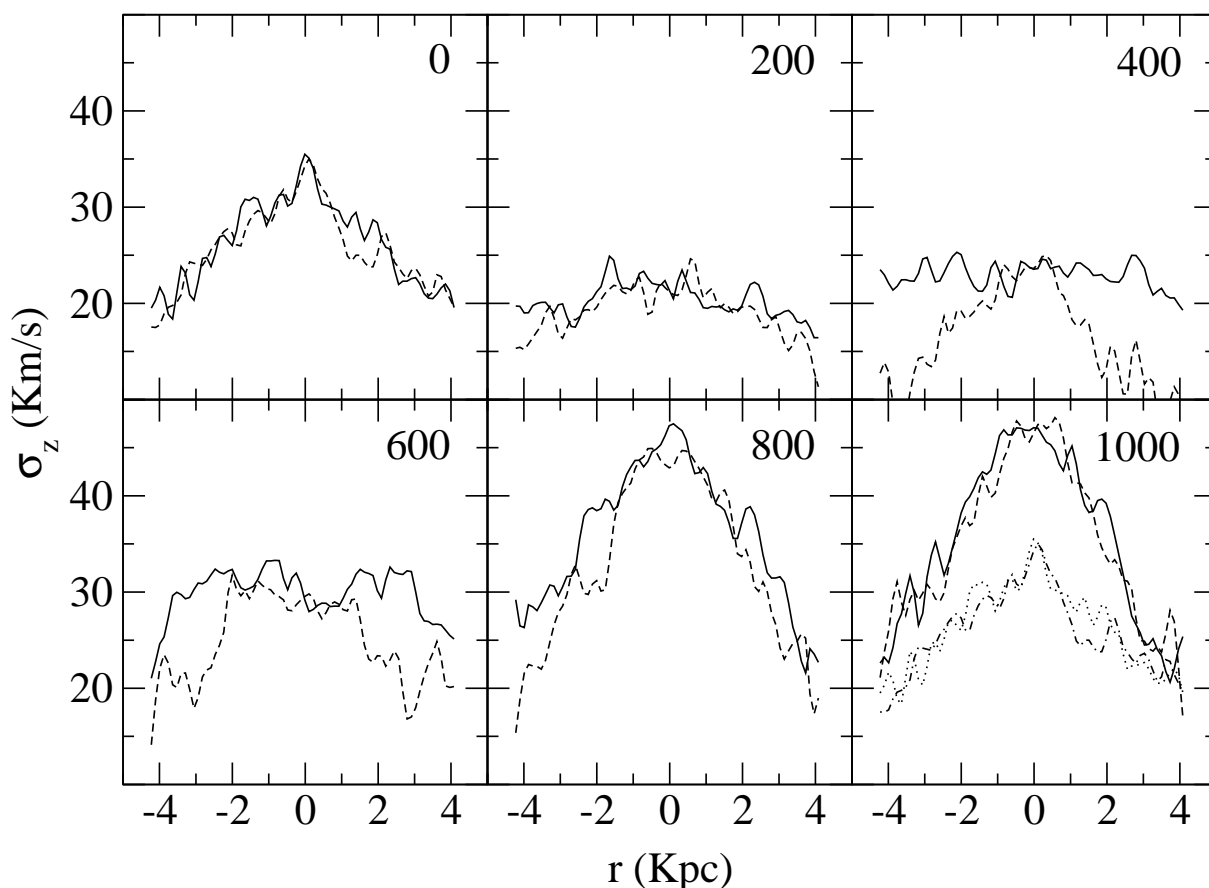


Fig. 12.— Radial profiles of the vertical velocity dispersion along the bar major axis (solid line) and minor axis (dashed line), as measured from simulated long slit spectroscopy, in our representative stellar disk numerical simulation. The corresponding times in virial units are displayed in the top right of each panel. The last panel corresponds to 2 Gyr of evolution. In the last panel we plot the initial profiles again, as a dotted line for the major axis and as a dash-dotted line for the minor axis, for comparison.